

# Extratropical circulation associated with Mediterranean droughts during the Last Millennium in CMIP5 simulations

Woon Mi Kim<sup>1,2,3</sup>, Santos J. González-Rojí<sup>1,2</sup>, and Christoph C. Raible<sup>1,2</sup>

<sup>1</sup>Climate and Environmental Physics, University of Bern, Bern, Switzerland

<sup>2</sup>Oeschger Centre for Climate Change Research, University of Bern, Bern, Switzerland

<sup>3</sup>Now at: National Center for Atmospheric Research, Boulder Colorado, United States

**Correspondence:** Woon Mi Kim (wmikim@ucar.edu)

## Abstract.

~~Knowing that internal climate variability is the principal driver of Mediterranean droughts during the last millennium, in this study, we investigate~~

The Mediterranean region is expected to experience significant changes in hydroclimate, reflected in increases in the duration and severity of soil moisture droughts. While numerous studies have explored Mediterranean droughts in coupled climate models under present and future scenarios, understanding droughts in past climate simulations remains relatively underexplored. Such simulations can offer insights into long-term drought variability that observational records cannot capture. Therefore, our study investigates circulation patterns in the Euro-Atlantic domain associated with multi-year soil moisture droughts over the Mediterranean region during the last millennium (850–2005 CE) in CMIP5-PMIP3 and CESM-LME simulations. ~~The focus is on the natural variability of droughts during 850–2005, thus excluding~~ Primarily, we examine the differences among the models in representing drought variability and related circulation patterns. For the analysis, we exclude the anthropogenic trends from ~~1850 CE onward. The results~~ 1850–2005 CE, and to detect the circulation patterns, we perform k-mean clustering combined with linear correlation analyses.

The findings re-confirm that Mediterranean drought occurrence during the last millennium is associated with internal variability. ~~In terms of the temporal variability, all~~ of the climate system. Drought variability, the associated circulation patterns, and the frequencies of these patterns vary across the models. Some climate models exhibit a multi-decadal anti-phase occurrence of ~~droughts some drought periods~~ between the western and eastern Mediterranean agreeing regions, although the exact periods of coherence differ among the models. This anti-phase co-variability, which agrees with some proxy records. ~~This anti-phase occurrence of droughts,~~ can be explained by the dominant circulation patterns in each region detected by the models: western Mediterranean droughts are dominated by a high-pressure system ~~and ridge~~ over central Europe and an NAO-like a North Atlantic Oscillation (NAO)-like pattern, while eastern Mediterranean droughts are linked to positive pressure anomalies in the southern and eastern Mediterranean, negative NAO, ~~negative EA and EA-WR-like patterns. However,~~ Eastern Atlantic, and Eastern Atlantic-Western Russia-like patterns. The frequencies of these modes of climate variability are strongly model-dependent, i.e. ~~each model has its preferred circulation patterns that,~~ some patterns occur more frequently ~~during droughts or~~ only in some models, suggesting that the main drivers of droughts differ ~~between among~~ the models. The models' preference

~~is therefore a potential~~ Although it is complicated to evaluate the representation of droughts and associated circulation among the models, in general, the models with lower horizontal and vertical spatial land resolutions exhibit drought variability and patterns that distinctly differ from other models. These model differences and preferences toward some circulation patterns can be a source of uncertainties in ~~Mediterranean droughts in the~~ model-proxy comparison ~~and may have implications for of~~ Mediterranean droughts and potentially influence future climate projections.

## 1 Introduction

Droughts are recurrent climate events in the Mediterranean region where precipitation shows a high spatial and interannual variability (Lionello et al., 2006). The complex spatial and temporal characteristics of Mediterranean precipitation and hydroclimate are due to its geographical location, extending latitudinally from the semi-arid subtropics to temperate mid-latitudes; ~~and strong seasonal influences~~. The region is influenced by seasonal variations of the subtropical high in the Atlantic Ocean ; ~~teleconnections, and large-scale modes of variability and other teleconnection patterns~~ (Rodwell and Hoskins, 1996; Krichak and Alpert, 2005; Lionello et al., 2006). ~~The climate of~~ While considerable spatial and temporal variability exists across the Mediterranean region, the climate is characterized by a wet ~~winter and hot dry summer, receiving a cold season and a dry hot season~~ (Xoplaki et al., 2004; Lionello et al., 2006). The wet cold season, typically extending from fall to spring, is a crucial ~~period for moisture supply, where a~~ large proportion of precipitation ~~originated from the is provided by~~ mid-latitude circulations and westerlies ~~during the winter (Lionello et al., 2006). Hence, winter is the crucial season for moisture supply that determines the intensity of drought impacts~~. Therefore the season dictates the intensity and impacts of droughts on the region.

Although droughts are natural fluctuations of ~~this the~~ region with highly variable seasonal hydroclimate conditions, ~~future climate~~ the Mediterranean region is a climate hotspot that will experience strong hydroclimate change (Giorgi, 2006; Cook, 2020) Future climate projections indicate robust increases in drought frequencies and intensities over the Mediterranean region even under stricter mitigation scenarios (~~Lehner et al., 2017; Samaniego et al., 2018; Masson-Delmotte et al., 2021~~) (~~Lehner et al., 2017; Cook,~~ 2020). This change is principally attributed to the intensification of the global hydrological cycle caused by anthropogenic influences in the atmosphere (~~Masson-Delmotte et al., 2021~~) (Douville et al., 2021). In the ~~Mediterranean~~ region, precipitation is expected to decrease due to an expanding Hadley Cell (Previdi and Liepert, 2007) and a poleward shift of the mid-latitude storm tracks (Yin, 2005; Wu et al., 2011). The most significant change will occur in the winter precipitation and its associated circulation, ~~which is~~ partially contributed by a decrease in the regional land-sea temperature gradient (Tuel and Eltahir, 2020). In addition to that, the future increase in temperature will amplify land-atmosphere ~~feedbacks and vapour~~ feedback and vapor pressure deficit, which will potentially enhance the intensity of droughts (Zhou et al., 2019).

Up ~~to date~~ until now, circulations associated with future potential changes in hydroclimate, including persistent droughts ~~are,~~ have been extensively studied in the region (e.g., Dubrovský et al., 2014; Spinoni et al., 2020; Tramblay et al., 2020; Cos et al., 2022). However, how drought-associated circulations ~~look like~~ looked before the anthropogenic greenhouse gas (GHG) era ~~is comparably less explored~~ remains comparably underexplored. Long past climate data enable us to examine persistent droughts, which are the conditions that can ~~possibly~~ be comparable to the future drying over the region, and their long-term variability

that cannot be captured in the limited-length observational-based records. Among the past periods, the last millennium is of particular interest as it is a relatively close ~~time~~-period with no ~~strong change in climate boundary conditions~~ substantial change in external forcing and with abundant high-quality proxy-based reconstructions (PAGES Hydro2k Consortium et al., 2017).

Several ~~natural~~-proxy-based reconstructions of past hydroclimate have contributed to a better understanding of ~~droughts~~ drought variability and their associated climate modes during the last millennium (PAGES Hydro2k Consortium et al., 2017). One of the widely used proxy-based datasets is a tree ring-based reconstruction of summer ~~dry-dryness~~ and wetness in Europe, known as the Old World Drought Atlas (OWDA; Cook et al., 2015). Using OWDA, Cook et al. (2016) identified a ~~multi-decadal~~ multidecadal in-phase drought occurrence across the Mediterranean basin and an anti-phase occurrence within the eastern Mediterranean. This result contradicts the finding by Roberts et al. (2012) based on the lake sediment records, which have shown an anti-phase hydroclimate variability between the western and eastern Mediterranean from the Medieval Climate Anomaly period. Different proxy-based studies have indicated that the Mediterranean hydroclimate's variability is influenced by several modes of climate variability and atmospheric circulation, such as Eastern Atlantic Pattern (EA; Cook et al., 2015), and North Atlantic Oscillation (NAO; Cook et al., 2015; Baek et al., 2017; Markonis et al., 2018). In a long-term analysis for the entire last millennium, Markonis et al. (2018) found that over southern Europe, including the Mediterranean, drier conditions have become dominant in the 20th century exceeding the millennial hydroclimate boundaries. Regarding natural external forcing, volcanic eruptions that are the natural radiative forcing with the strongest impact on the global climate during the last millennium, have caused wetter conditions that last up to a few years after the first emissions (Gao and Gao, 2017; Rao et al., 2017).

Besides proxy-based reconstructions, fully-coupled climate models have been useful tools to support findings from proxy-based studies. Since climate simulations can cover the temporal resolutions and time periods that go beyond the time scales of proxy records, they can ~~provide more insight into~~ allow us a broader exploration of the variability and mechanisms of past hydroclimate and droughts. For instance, the impact of volcanic eruptions on long-lasting droughts ~~was has been~~ assessed on a global scale (Stevenson et al., 2017) and the Mediterranean region (Kim and Raible, 2021) using the Community Earth System Model (CESM; Lehner et al., 2015; Otto-Bliesner et al., 2016). ~~With the same model~~ In the latter study, Kim and Raible (2021) found that persistent Mediterranean droughts in the last millennium are associated with modes of internal climate variability, with a strong influence of positive NAO and higher than normal regional temperatures in a CESM1 simulation. Other studies ~~come to the same conclusion, e. g. have drawn a similar conclusion~~ Using simulations from the CCSM4 and MPI-ESM climate models, Xoplaki et al. (2018) showed that ~~changes~~ multidecadal variations in the eastern Mediterranean hydroclimate are explained by internal ~~variability in CCSM4 and MPI-ESM simulations. They also found that the type of internal variability is model-dependent~~ climate dynamics. By comparing three historical periods with large hydroclimate events over the region, they found notable differences in the climate patterns during the same periods between the two models. The observed discrepancies in climate patterns and timing of hydroclimate events between the models, and also between the models and the proxy records, indicate that exact temporal and spatial agreement of events between climate models and proxy records cannot be expected.

Despite these past studies on the Mediterranean hydroclimate, temporal variability and circulation patterns associated with multi-year persistent droughts during the last millennium are ~~still~~ not fully explored in currently available climate simulations.

If internal variability is an important driver of droughts before the pre-industrial period, it is necessary to understand which modes of climate variability or circulation patterns are involved in each climate model, and whether these patterns are depicted in the same way in all model simulations. Therefore, the objective of this study is to examine how different coupled climate models depict the temporal variability of droughts and associated circulation patterns during the last millennium. Additionally, we evaluate the differences among the models in representing drought-related circulations. The focus of this study is on the patterns in the mid-latitudes mid-latitude circulations patterns that have more impacts on the Mediterranean hydroclimate. In this study, we examine extratropical (Xoplaki et al., 2012; Kim and Raible, 2021). We examine circulation patterns in the Euro-Atlantic domain associated with the western (12°W–19°E, 32°–43°N) and eastern (19°–37°E, 32°–43°N) Mediterranean droughts during the last millennium (850–2005) CE using the model simulations from the fifth phase of the Climate Model Intercomparison Project (CMIP5; Taylor et al., 2012) - Paleoclimate Model Intercomparison Project Phase 3 (PMIP3; Schmidt et al., 2012) and CESM Last Millennium Ensemble Project (CESM-LME; Otto-Bliesner et al., 2016).

All the details of the datasets are provided in Section 2. Soil moisture anomalies are employed as a drought metric in this study, and commonly used statistical techniques in climate sciences are applied to detect circulation patterns. The information about these methods is presented in Section 3. Drought periods and main circulation patterns are identified in the climate model simulations and compared to each other in Section 4. This study ends with a discussion of the results in Section 5, followed by the concluding remarks in Section 6.

## 2 Data

### 2.1 CMIP5-PMIP3 model simulations

To study drought variability and the associated extratropical circulation patterns during 850–2005 CE, we use several forced transient simulations of Last Millennium (LM; 850–1850 CE) and historical period (Hist; 1850–2005 CE) from the CMIP5-PMIP3 (Schmidt et al., 2012; Taylor et al., 2012) and CESM-LME projects. We (Otto-Bliesner et al., 2016). Our focus is on droughts that affect deep soil moisture conditions, known as soil moisture droughts (Dai, 2011). Therefore, we consider only simulations that provide the vertical water content of each soil layer (variable names *mrlsl* in PMIP3-CMIP5, and *SOILLIQ* and *SOILICE* in CESM-LME). Thus With this criterion, only four climate model simulations models are used for the analysis: GISS-E2-R, CCSM4, bcc-csm1-1, and MIROC-ESM. For CESM-LME, we use 12 ensemble members of CESM1 from members 2 to 13 available in <https://www.earthsystemgrid.org>. The vertical water content of soil layers up to 70 cm depth is employed to quantify soil moisture droughts. Surface temperature and geopotential height at 500 hPa are retrieved to describe the mean temperature and circulation conditions during the Mediterranean drought years. All variables have a monthly temporal resolution, but different horizontal and vertical land resolutions, as shown in Table 1. Additional specifications of each model are summarized there. All simulations are transient that were run with the volcanic, solar, and greenhouse gas (GHG) forcings of 850–2005 CE agreed upon by the PMIP3-CMIP5 protocol (Schmidt et al., 2012; Taylor et al., 2012). For GISS-E2-R in the LM experiment, three realizations (*ilr1p122*, *ilr1p125*, and *ilr1p128*) that were run with the same volcanic forcing are considered in the analysis.

**Table 1.** Details of the [CMIP5-PMIP3 \(Schmidt et al., 2012; Taylor et al., 2012\)](#) and [CESM-LME \(Otto-Bliesner et al., 2016\)](#) climate models and simulations used for the analysis. LM and Hist indicate the last millennium and historical experiments, respectively.

~~Model Horizontal resolution Vertical soil layers up to 70 cm LM Hist West East CESM1 12 12 1.875° × 2.5° 7 85 46~~  
~~GISS-E2-R 3 3 2° × 2.5° 7 85 46~~  
~~CCSM4 1 3 1° × 1.25° 7 173 99~~  
~~bcc-csm1-1 1 3 2.8° × 2.8° 7 38 25~~  
~~MIROC-ESM 1 3 2.8° × 2.8° 3 22 12~~

Model	Number of Ensemble Members		Land model	Horizontal resolution of the land model	Vertical soil layers up to 70 cm	Number of grid points		Reference
	LM	Hist				West	East	
CESM1	12	12	CLM4	1.875° × 2.5°	7	85	46	Otto-Bliesner et al. (2016)
GISS-E2-R	3	3	ModelE Land surface model	2° × 2.5°	3	42	24	Schmidt et al. (2014)
CCSM4	1	3	CLM4	1° × 1.25°	7	173	99	Gent et al. (2011)
bcc-csm1-1	1	3	BCC-AVIM1.0	2.8° × 2.8°	7	38	25	Wu et al. (2014)
MIROC-ESM	1	3	MATSIRO + SEIB-DGVM	2.8° × 2.8°	3	22	12	Watanabe et al. (2011)

## 2.2 Observation-based data

Since observations of subsurface soil moisture content are spatially scarce, we use soil moisture content from the Noah land surface model (NOAH-LSM), which is a part of the Global Land Data Assimilation System ~~2.1 (GLDAS2.1; Rodell et al., 2004)~~  
130 [2.0 \(GLDAS2.0; Rodell et al., 2004\)](#). NOAH-LSM is a physical land model that solves and quantifies the transfer of heat and moisture at the surface to the subsurface levels and interactions between the soil, atmosphere, and vegetation. The model is forced by atmospheric conditions from satellite- and ground-based observational data products. The soil moisture variable from NOAH-LSM has four layers ~~up to that extend to a depth of~~ two meters, with monthly temporal and 1° spatial resolutions extending from 1948 to the present.

135 To characterize the atmospheric circulation, we use the monthly mean geopotential height at 500 hPa from the ERA5 reanalysis (Hersbach et al., 2018, 2020). ERA5 is the latest reanalysis product of the European Centre for Medium-Range Weather Forecasts (ECMWF), and the products are generated with the 2016 version of the ECMWF numerical weather prediction model and the integrated forecasting system Cy41r2 data assimilation. The spatial resolution of ERA5 is 0.25° and the temporal extent is from 1950 to the present. For the analysis, ERA5 data is horizontally interpolated to 1° spatial resolution to  
140 [match the resolution of NOAH-LSM. We use the NOAH-LSM land variable instead of the one from ERA5, as NOAH-LSM is forced with the biases-corrected observation-based datasets. Therefore, NOAH-LSM could be a better choice that reflects more realistic present-day soil moisture variability.](#)

### 3 Methods

#### 3.1 Calculation of anomalies

145 The following variables from the NOAH-LSM, ERA5, and climate simulations are used in the analysis: the surface temperature, geopotential height at 500 hPa, and soil moisture content at of vertical soil layers. ~~These variables are transformed into the annual mean anomalies at each grid point. We use annual mean anomalies in order to include winter conditions in the analysis, as it is an important season for the annual hydroclimate in the Mediterranean. Prior to the anomaly calculation, the~~ The soil moisture content of soil layers from NOAH-LSM and the climate models are vertically integrated to 70 cm. If the exact 70 cm  
150 level is ~~not available, unavailable, a linear interpolation is applied to estimate~~ the vertically integrated soil moisture ~~is linearly interpolated over depth to the 70 cm content at that~~ level.

~~Then, first, the monthly~~

The variables are all transformed into annual mean anomalies. Wet seasons are critical periods for the moisture supply of the region, and therefore, when strong circulation patterns take place (Xoplaki et al., 2004; Lionello et al., 2006). Therefore,  
155 we use annual mean anomalies to capture the mean variability of hydroclimate throughout the entire year instead of focusing on some particular seasons, i.e., summer growing seasons. This is to include the influences of wet seasons, which is the crucial season for moisture in the region, in the analysis. The annual mean anomalies are calculated by subtracting the multi-year ~~monthly means from each of the monthly values. Different reference periods for the means from the annually averaged time series. Depending on the data set and the experiment, different reference periods are used to calculate the~~ multi-year ~~monthly means are used depending on the periods of study and experiments~~ means. For the ~~observational-based~~ observation-based data, NOAH-LSM and ERA5, the reference period is 1950–1979 CE. For the LM and Hist experiments in the climate models, the ~~period 850–1849 is used. Second, the necessary annual mean anomalies are obtained by averaging these monthly anomalies annually. reference period is 850–1849 CE.~~

In ~~addition~~ the next step, we remove the strong unprecedented trends in the Hist simulations (1850–2005). ~~Thereby, CE).~~  
165 This means that the effects of increased GHG on droughts is not included in the analysis. To achieve this, we calculate the ensemble means of the ~~anomalies are calculated and subtracted~~ annual anomalies for each climate model during the period 1850–2005 CE. Then, for each model, we subtract their corresponding ensemble mean from each of the ensemble member anomalies ~~at each grid point employing~~. The approach follows a similar method to Maher et al. (2018). ~~This method guarantees that only internally driven variability remains in the time series of the variables. This,~~ which aims to exclude a trend caused  
170 by increasing anthropogenic GHG concentration from a time series. Note that the method is not applied to the LM period, therefore, the ~~LM anomalies~~ anomalies during LM still contain forced signals such as those from volcanic eruptions. ~~Note that the~~ The number of ensemble members can have an influence on the final output of Hist. The potential implications of this method are discussed in Section 5.

~~The two periods, LM and Hist, are merged into one time series, and droughts are estimated for each of the models and~~  
175 ~~regions. The number of drought years is counted with a moving window of a century, and a percentage of total drought years~~

~~(years with droughts in all ensemble members divided by the total model years) and a mean duration of droughts are calculated for each of the models and regions.~~

### 3.2 Region of study

Similar to Cook et al. (2016), we separate the Mediterranean into two subregions: the western Mediterranean encompassing 13°W–19°E, 32°–43°N and the eastern Mediterranean occupying 19°–37°E, 32°–43°N. The separation is motivated by the suggested influences of the circulation patterns over the Mediterranean region (Düneloh and Jacobeit, 2003; Lionello et al., 2006), such as the NAO, ~~EA, East Atlantic (EA), and Eastern Atlantic-West Russian (EA-WR), and the Scandinavian patterns.~~ The western Mediterranean is more intensely influenced by NAO than the eastern region, and the eastern region is not only affected by NAO but also strongly linked with East Atlantic-type patterns.

### 185 3.3 Comparison between present-day observation-based data and model simulations

Pearson correlation coefficients (PCC) are calculated between the annual soil moisture anomalies (SOIL) of the western and eastern Mediterranean ~~;~~ and the geopotential height anomalies (Z500) in the north Atlantic and European domain (70°W–70°E, 21°–85°N). SOIL is from NOAA-LSM and Z500 from ERA5, both obtained from Section 3.1. The PCC allows us to measure the link between ~~the~~ soil moisture variability and circulations in the present day. The period for the correlation is 56 years from 1950 to ~~2005–2005 CE.~~ Assuming that NOAA-LSM ~~represents realistically~~ realistically represents soil moisture variability, the correlation patterns of other climate models are compared against the pattern of NOAA-LSM.

In addition, to quantify the spatial similarity of the correlation patterns, PCC is calculated between the correlation pattern NOAA-LSM–ERA5 for the western and eastern regions separately and the patterns of each climate model. For this spatial comparison of the correlation patterns, the horizontal resolutions of all data are interpolated to match those of the coarser climate models, which are bcc-csm1-1 and MIROC-ESM (Table 1). This PCC would provide a numerical value to evaluate the overall resemblance between the present-day NOAA-LSM–ERA5 field and the climate models.

### 3.4 Drought definition

The annual anomalies of vertically integrated soil moisture at 70 cm (SOIL) in LM and Hist are used as the metric to quantify annual droughts. The 70 cm level is a deep soil level that can reflect the impacts of soil moisture change on vegetation and ecosystems, hence, ~~better representing~~ better representing soil moisture droughts, including their persistent characteristics (Dirmeyer, 2011; Ghannam et al., 2016; Esit et al., 2021).

Two temporal and spatial criteria are applied to detect droughts over each of the study regions:

- i) We combine two definitions used by Kim and Raible (2021) and Coats et al. (2013): a drought must be composed only of negative SOIL (Kim and Raible, 2021), and it must commence after two consecutive years of negative SOIL and continue until two consecutive years of positive anomalies (Coats et al., 2013). Thereby, we ensure that droughts are intense enough as they are composed of only negative values without being interrupted by a particularly wet year in

between. This definition also assures a minimum drought duration of two years. Using these definitions, droughts are detected at each horizontal grid point in the study regions.

210 ii) A spatial restriction is applied to the detected drought years to be considered as a regional-scale drought (western or eastern). At least 60% of ~~the all~~ horizontal grid points ~~over the~~ (which is approximately from 56% to 61% of the areal extent) within the region (the western or eastern Mediterranean) need to be under negative SOIL conditions during all consecutive drought years. This ~~guarantees that~~ criterion ensures that a substantial portion of the region experience drought conditions and ensures that droughts are regional and not local events.

~~When these temporal and spatial criteria are fulfilled, droughts are identified for all grid cells.~~ At this step, we do not  
215 apply any horizontal interpolation in SOIL. Thus, regional coverage (geographical extension and number of grid cells) differs slightly between the models (as shown in Table 1). Nevertheless, this approach avoids changes in the initial SOIL values, as hydroclimate variables associated with precipitation can be sensitive to the horizontal grid resolution (Champion et al., 2011; Kopparla et al., 2013; Haren et al., 2015). Also, in this way, the effects of the number of land grid cells on drought estimation and drought-associated circulation can be identified. ~~Next, the weighted spatial average of SOIL is calculated to generate a~~  
220 ~~time series for the western and eastern Mediterranean.~~

Finally, a drought is considered regional (only west- or east-occurring) when the temporal overlap during one drought event between the two regions is less than 50%. When the temporal overlap is more than 50%, the event is considered a pan-Mediterranean drought. The analysis focuses on only west and east-occurring droughts. ~~The, and the~~ reason is that pan-Mediterranean droughts are rather rare events to occur.

225 When these temporal and spatial criteria are fulfilled, droughts are identified for the west and east Mediterranean separately. The frequencies of droughts, in terms of the number of drought years, are estimated during the entire 850–1850 CE by combining the SOIL of LM and Hist experiments for each of the models and regions. The number of drought years is counted with a moving window of a century, and a percentage of total drought years (years with droughts divided by the total model years) and a mean duration of droughts are calculated for each of the models and regions. Also, the time series of SOIL  
230 is generated by applying spatial weights to the soil moisture anomalies, taking into account the spatial extent of each grid cell within the confined region. The means and the standard deviations of SOIL during LM and Hist are calculated, and the values are compared among the models. ~~Only climate models with some ensemble members in LM, such as CESM1 and GISS-E2-R, show few numbers of pan-Mediterranean droughts. Other models only present one or two drought events with Pan-Mediterranean characteristics. In the Hist simulations, when the anthropogenic signals are removed (Section 3.1),~~  
235 ~~pan-Mediterranean droughts are not detectable.~~

We perform wavelet coherence (Grinsted et al., 2004) on the time series of the number of droughts and the soil moisture anomalies between the west and east Mediterranean. The purpose is to assess the phase relationship, dominant frequencies, and temporal variations of correlations in soil moisture anomalies and drought occurrences between these two regions.



### 3.5 Extratropical circulation pattern detection: principal component, k-mean clustering and Pearson correlation

240 analyses

Drought-associated circulation patterns are detected in the ~~model simulations using simulations using the geopotential height anomalies at 500 hPa (Z500)~~ over 70°W–70°E, 21°–85°N during drought years. All Z500 fields are interpolated to a common horizontal resolution of CESM1 (Table 1).

The method for pattern detection consists of a combination of ~~several~~ standard statistical methods in climate sciences: a principal component (PCA), k-mean clustering (KCA), and Pearson correlation ~~analysis analyses~~ (PC-KCA-PCC method). The flow chart in Fig. 1 illustrates all the steps from the definition of drought (step 1, Section 3.4) to the detection of associated circulation patterns.

~~After obtaining~~ A detailed explanation of the method is as follows: ~~after obtaining all~~ drought years in ~~step~~ Step 1, in ~~step~~ Step 2 ~~the PCA technique~~, PCA is applied to the Z500 ~~fields~~. ~~PCA allows a decomposition of anomalies of the drought~~ years. PCA is employed to increase the performance of KCA in the next step, which is the primary tool for detecting circulation patterns in this study. ~~PCA decomposes~~ a spatio-temporal field  ~~$X(t, s)$  into spatial patterns  $u_k(s)$  ( $s$  being  $X(t, l)$  using spatial functions  $u_i(l)$ , where  $l$  is the spatial dimensions ) and its associated temporal indices  $T_k(t)$  (latitude  $\times$  longitude in our study), and their associated temporal functions  $T_i(t)$ , where  $t$  is the time steps , here years ) for a in years ( $t$  is the total drought years), in  $M$  number of modes  ~~$M$  contained in the field (Hannachi et al., 2007)~~ or principal components (PCs; Hannachi et al., 2007). PCA is based on the following equation:~~

$$X(t, sl) = \sum_{k=1}^M \sum_{i=1}^M T_{ki}(t) \cdot u_{ki}(sl) \quad (1)$$

PCA ~~provides generates~~ a new set of uncorrelated linear combinations of the original field (~~principal components; PC~~) that captures its original variance. ~~Each PC has an associated referred to as principal components PCs, represented as  $T_i(t) \cdot u_i(l)$  in eq. 1). These components capture most of the original variance, and each PC is associated with a progressively decreasing explained variance. By truncating the number of PCs according to a certain threshold , PCA can serve as a tool to filter the original data by reducing the dimension of of explained variance, PCA reduces the dimension of a multi-dimensional dataset (Monahan et al., 2009). In data set (Hannachi et al., 2007). For this study, PCA is applied to the Z500 fields during droughts for each model, experiment — LM or Hist —, and region — the western or eastern Mediterranean. The minimum threshold considered for the we consider a threshold of 70% of the total explained variance for the truncation of PCs is 70%. The truncation reduces substantially. The method substantially reduces the number of retained PCs from the total number  $M$  to  $N$  and increases, thereby enhancing the performance of KCA in the next step. The resulting new PC field of Z500 has a spatio-temporal dimension of  $N \times t$ , with  $t$  being the total droughts.~~

In ~~step~~ Step 3, KCA is applied to the ~~fields of PCs to detect the characteristic circulation patterns during droughts~~  $N \times t$  PC field to detect similar patterns among  $t$  drought years and group them together. KCA is an unsupervised classification technique that aims to cluster variables ~~by their similarities minimizing the based on their similarities, minimizing the geometrical distance~~ between the data points  $x_i$  and between the potential clusters  $c_k$  (Wilks, 2011; Zscheischler et al., 2012). Hence, it attempts to

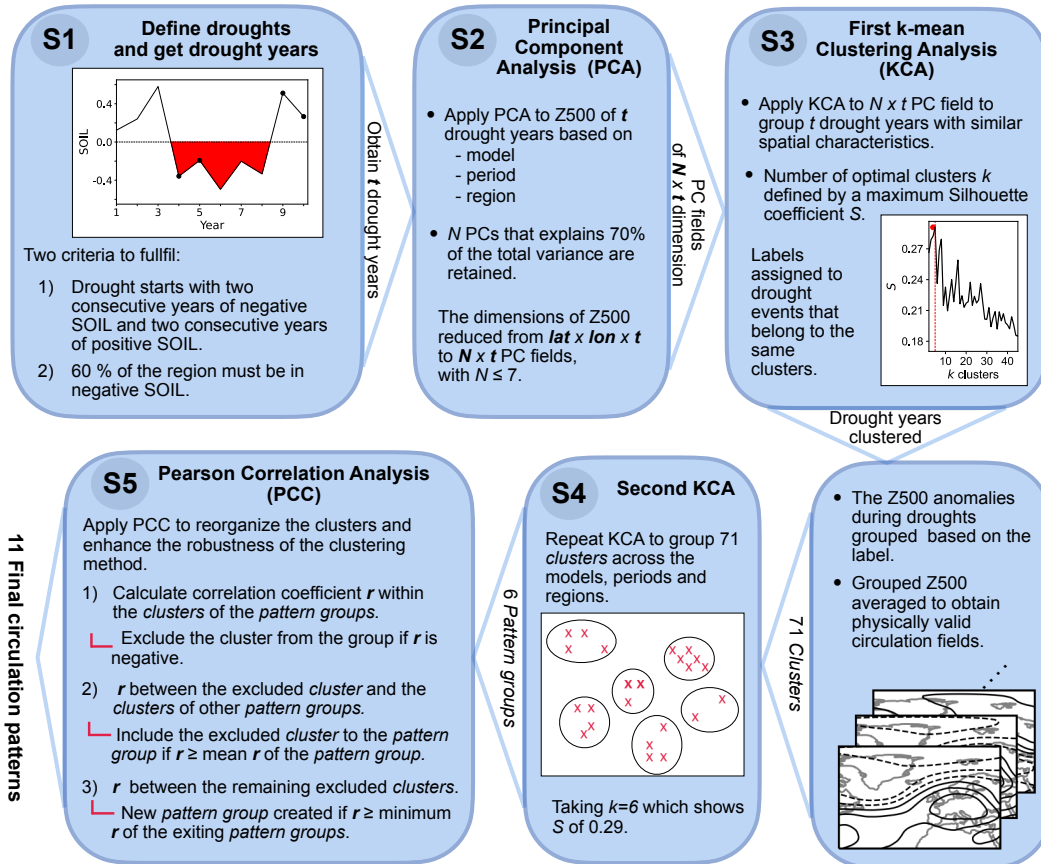


**Figure 1.** Flow chart summarizing the procedure for detecting the ~~detection of the~~ extratropical circulation patterns associated with the Mediterranean droughts. The diagram includes the following steps: S1) define droughts and get the ~~definition of~~ drought years, S2) apply the principal component analysis to Z500, S3 and S4) apply the K-mean clustering analysis to the PC fields and the temporarily clustered circulation patterns (clusters), and S5) perform the Pearson correlation analysis to obtain the final circulation patterns. Note that the figures in S1, S3, and S4 are included for illustrative purposes. A detailed description of each step can be found in Sections 3.4 and 3.5.

minimize the clustering objective function  $Q$  by

$$Q(c_1, \dots, c_k) = \frac{1}{n} \frac{1}{t} \sum_{i=1}^{nt} \min_{k=1, \dots, k} \|x_i - c_k\|^2 \quad (2)$$

where  $k$  is the number of clusters and  $n$  is the number of data points, and  $t$  is the total data points, which in this study are the drought years. KCA has the advantage of repeating the calculation in equation estimation in eq. 2 until the best set of  $k$  number of clusters is found. The number of PCs

The numbers of PC  $N$  and clusters  $k$  is not determined are not defined in the beginning. We calculate the mean Silhouette coefficients  $S$  (Shahapure and Nicholas, 2020) for a range of  $N$  and  $k$  to find the optimal  $N$  and  $k$  (step Step 3 in Fig. 1). A mean Silhouette coefficient  $S$  is a metric that measures the quality of clustering by considering the similarity within the same cluster and the dissimilarity between the clusters. To get the mean Silhouette coefficient  $S$ , a Silhouette coefficient  $s$  for each data point is first calculated by

$$s = \frac{b - a}{\max(a, b)} \quad (3)$$

where  $a$  is the mean distance within the same cluster, and  $b$  is the mean distance to the nearest neighbouring neighboring cluster. All the  $s$  for each point are averaged to obtain  $S$ .  $S$  ranges between -1 and 1, 1 indicating an optimum cluster showing with a high similarity between among its elements and a high distance to the neighbouring clusters. from the neighboring clusters.  $S$  are calculated across a range of  $N$  (with a minimum of 70% explained variance) and  $k$ . Then, the  $N$  and  $k$  with yielding the highest  $S$  are selected. Following this, PC-KCA is applied to the  $N \times t$  PC field with a parameter  $k$  for the number of clusters.

Through this PC-KCA process, 71 clusters are obtained, which characterize drought years with similar spatial characteristics are identified and grouped, with labels assigned to the events that belong to the same cluster. Subsequently, to retrieve circulation fields of physical significance, the Z500 during droughts for each model, period and region. anomalies during droughts are grouped together based on the label assigned by the PC-KCA process. Then, the averages of these grouped Z500 anomalies are computed for each group to obtain clusters that represent drought circulation patterns.

The PC-KCA procedure is performed for each model — CESM1, GISS-E2-R, CCSM4, bcc-csm1-1, and MIROC-ESM —, experiment — LM or Hist —, and region — western or eastern Mediterranean — separately. After Step 3, in total, 71 clusters are obtained. The  $N$  number of PCs, the explained variance explained by the PCs, the each PC, the  $k$  number of clusters, and the mean Silhouette coefficients  $S$  obtained during the PC-KCA steps can be found in Table 2. The supplement to this paper includes the full range of silhouette coefficients Silhouette coefficients  $S$  obtained for each model and period (LM and Hist simulations in Fig. S1 and Fig. S2, respectively).

In step

In Step 4, KCA is applied once again to these 71 clusters (from now on, referred to as cluster) are re-clustered through KCA and Pearson correlation analysis in order to gather similar clusters between all the models, periods to group similar clusters across all models, experiments, and regions (steps 4 and 5 in Fig. 1, respectively). After that, we will define the final groups of drought-associated circulation patterns (from now on, pattern group). For this, first, KCA is applied to the 71 clusters to get

**Table 2.** Percentages of variance explained by  $N$  number of principal components (PC),  $k$  number of clusters, and mean Silhouette coefficients  $S$  obtained by the PC-KCA steps of the pattern detection according to the model, Mediterranean region and period considered.

Model	Region	Last Millennium (LM)			Historical (Hist)		
		% Variance ( $N$ PC)	$k$ Clusters	$S$ Coefficient	% Variance ( $N$ PC)	$k$ Clusters	$S$ Coefficient
CESM1	West	77.91 (5)	3	0.17	79.82 (5)	3	0.23
	East	78.60 (5)	3	0.18	79.82 (5)	3	0.20
GISS-E2-R	West	75.11 (5)	3	0.19	75.78 (5)	7	0.22
	East	73.63 (6)	3	0.17	77.60 (5)	3	0.22
CCSM4	West	77.03 (5)	4	0.18	80.20 (5)	3	0.18
	East	74.43 (5)	3	0.19	80.56 (5)	3	0.24
bcc-csm1-1	West	77.01 (5)	3	0.19	83.93 (5)	3	0.26
	East	75.34 (5)	6	0.19	80.95 (5)	3	0.23
MIROC-ESM	West	72.90 (5)	5	0.18	76.05 (5)	3	0.24
	East	75.13 (6)	3	0.17	79.85 (5)	4	0.19
Total 71 clusters							

305 ~~the temporary pattern groups.~~ Initially,  $k = 6$  is used as the mean Silhouette coefficient since  $S$  decreases abruptly (step after this  $k$  (Step 4 in Fig. 1). These six clusters obtained by grouping cluster are referred to as the pattern groups.

~~The final step~~In the final Step 5 assures the similarity between the clusters. Pearson correlation analysis (PCC) is performed on the clusters within the same pattern group (step 5 in Fig. 1). For this, we calculate and across different pattern groups to create new pattern groups based on the Pearson correlation coefficients  $r$  (PCC; Wilks, 2011) between the clusters of the same pattern groups. Within the same pattern group, if one cluster. This step is to ensure the similarity between the clusters within the same pattern group.

315 Initially, PCC is performed on the clusters within the six pattern group obtained in the previous step.  $r$  are calculated between all possible pairs of the clusters within a pattern group. Then, any cluster that is negatively correlated with one or more cluster members, this cluster-clusters of the same pattern group is excluded from the pattern group. The mean  $r$  of the pattern group is again calculated without the excluded clusters-group. Next,  $r$  is calculated between each excluded cluster and members-cluster and the clusters of the other pattern groups to determine if the excluded cluster can join a new pattern group. The criteria to join the pattern group is that the excluded cluster must show a five pattern groups. This is to determine whether the excluded cluster from one pattern group can join any of the other groups. The criterion for joining the other pattern group requires the excluded cluster to exhibit positive  $r$  with all cluster members-clusters of the target pattern group pattern group, and the  $r$  must be more than the minimum-mean  $r$  among the existing pattern of the target group. This process is repeated to all excluded clusters for all excluded clusters from the six temporary pattern groups-pattern groups.

320 If this reorganization of clusters-clusters is not successful for some excluded clusters-clusters,  $r$  is calculated between those clusters which are not-clusters which have not been assigned to any of the existing pattern groups. When some remaining clusters-six pattern groups. If some remaining clusters are positively correlated with each other with-and have a mean  $r$  of

325 ~~more-higher~~ than the minimum mean  $r$  among the ~~existing-pattern-group, they six pattern groups, these clusters~~ are gathered to  
~~create a new pattern group~~ form a new *pattern group*. This re-assignment is repeated until no ~~more-gathering-further grouping~~  
is possible. ~~This thorough process leaves-~~

Finally, ~~this thorough process results in 11 pattern-groups that represent the definitive pattern groups that~~ characterize  
~~the mean~~ circulation patterns associated with drought conditions in the Mediterranean region ~~-during the last millennium~~  
330 (850–2005 CE). The sequence of the PC-KCC-PCC technique involves the repetition of the clustering procedure three times.  
~~This procedure serves to enhance the robustness of the clustering method. This approach also allows us to trace clustered~~  
~~patterns throughout the entire procedure, exhibiting in each step the metrics ( $S$  and  $r$ ) that measure how well the patterns are~~  
~~grouped together.~~

~~Percentages of variance explained by  $N$  number of principal components (PC),  $k$  number of clusters, and mean Silhouette~~  
335 ~~coefficients  $S$  obtained by the PC-KCA steps of the pattern detection according to the model, Mediterranean region and period~~  
~~considered.~~

## 4 Results

### 4.1 Observation-model comparison (1950–2005 CE)

~~Fig. 2 shows SOIL~~ The annual soil moisture anomalies (SOIL) from NOAA-LSM and the ~~mean SOIL of five climate models~~  
340 ~~with the ensemble spread.~~ forced PMIP3-CESM1 simulations during 1950–2005 CE and 850–2005 CE over the Mediterranean  
~~region are presented in Fig. 2. SOIL during 850–2005 CE are standardized with respect to 850–1849 CE. During 1950–2005 CE~~  
~~(Fig. 2a), the variability of SOIL from NOAA-LSM is (the range of maximum and minimum over 1950–2005 CE is 18.29 mm~~  
~~month<sup>-1</sup>) is within the range of the CMIP5-PMIP3 model ensemble spread except for one year in 1975. The unprecedented~~  
~~trends in SOIL are clearly visible in the models from 1850 onward variability of the PMIP3-CESM1 model SOIL values~~  
345 ~~(the range of maximum and minimum across the models of 22.75 mm month<sup>-1</sup>). This observation indicates that the overall~~  
~~magnitudes of variability between the observation-based data and the models are comparable. However, the standard deviation~~  
~~( $\sigma$ ) of SOIL across the four models over the entire time (3.06 mm month<sup>-1</sup>) is lesser than the  $\sigma$  of SOIL of NOAA-LSM~~  
~~(4.37 mm month<sup>-1</sup>). This distinct  $\sigma$  indicates that there is some degree of discrepancies in SOIL variability among the models.~~  
~~GISS-E2-R, CESM1, and CCSM4 show  $\sigma$  of SOIL of 7.73, 5.44, and 4.43 mm month<sup>-1</sup>, respectively, which are higher than~~  
350 ~~that of NOAA-LSM, while bcc-csm1-1 and MIROC-ESM presents  $\sigma$  of 2.03, and 2.46 mm month<sup>-1</sup>, respectively.~~

~~The ensemble means of standardized SOIL during 850–1849 CE (Fig. 2band e). As described in Section 3.1, these trends~~  
~~were removed by subtracting from each of the ensemble members the anomalies at each grid point.)~~ shows no apparent  
~~monotonic trend during LM. In general, the ensemble means of each model exhibits decreases in SOIL since 1850 CE. The~~  
~~decreases are noticeable even considering the ensemble spreads of each model, except for MIROC-ESM. In MIROC-ESM,~~  
355 ~~a decline of SOIL is observed at the beginning of Hist, but then SOIL increases around 1950 CE. This trend of SOIL in~~  
~~MIROC-ESM is remarkably different from other models and may emphasize model-dependent response to forcing drivers,~~  
~~i.e., GHG forcing.~~

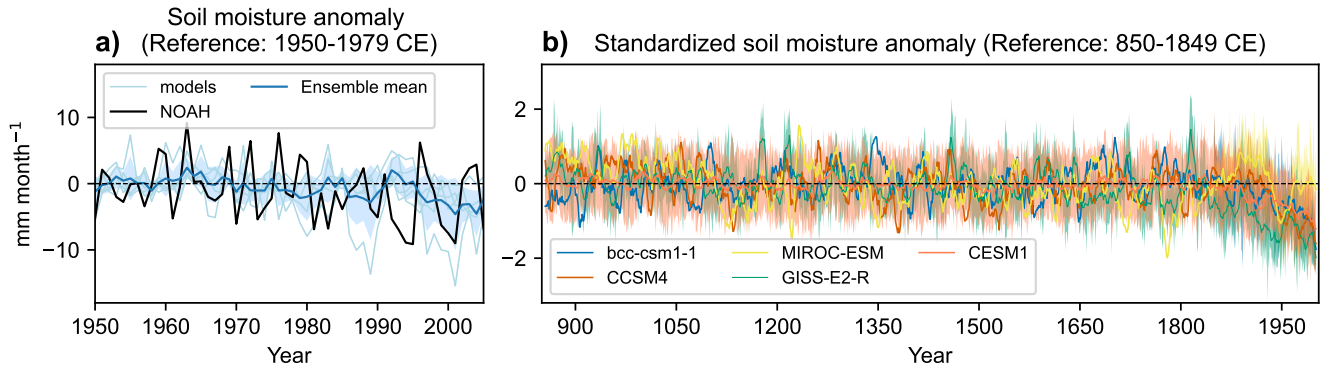


**Figure 2.** (a) The annual mean time series of SOIL over the Mediterranean region ( $13^{\circ}\text{W}$ – $37^{\circ}\text{E}$ ,  $32^{\circ}$ – $43^{\circ}\text{N}$ ) for the period 1950–2005 CE with respect to 1950–1979 CE. SOIL from NOAH-LSM is in black line and is in light blue from PMIP3-CESM1. Color shading indicates the ensemble spread denoted as one standard deviation ( $\sigma$ ) across the five climate models in Table 1. (b) 10-year running means (thick lines) and ensemble spreads (color-shaded) of standardized SOIL during 850–2005 CE with respect to 850–1849 CE, from the PMIP3-CESM1 transient LM and Hist simulations. Note that the post-1850 trends in Hist are not detrended in these time series.

The spatial correlations between SOIL and Z500 of ~~NOAH-LSM~~ NOAH-LSM-ERA5 and each of the climate simulations are presented in Fig. 3. In addition, the values of the correlation coefficients between these spatial correlation fields of  
 360 NOAH-LSM-ERA5 and each of the climate models are shown on the top of each panel. In all simulations, SOIL is negatively correlated with Z500 in the western (Fig. 3a) or eastern Mediterranean (Fig. 3b). This indicates that a decrease in SOIL is associated with a high Z500, which is a typical atmospheric circulation during dry conditions. A high-pressure system and a ridge over a region are associated with stable atmospheric conditions with a clear sky, low precipitation, and high temperature, which can. The latter can also induce an initial increase in evapotranspiration that accelerates a the loss of soil moisture. In  
 365 addition Additionally, the anticyclonic circulation hampers incoming moisture fluxes from the Atlantic. However, the spatial extent of these negative correlations centered on the focus regions varies across the models, and the signals of correlations outside of the regions differ noticeably between some models (e.g., CESM1 and bcc-csm1-1).

The annual mean time series of SOIL in the Mediterranean region ( $13^{\circ}\text{W}$ – $37^{\circ}\text{E}$ ,  $32^{\circ}$ – $43^{\circ}\text{N}$ ) with different reference periods: (a) from NOAH-LSM (blue line), and ensemble mean (dashed red line) and spread (shaded red; given as one standard deviation) of simulations included in Table 1 during 1950–2005 with a reference period of 1950–1979, (b) 10-year running means (lines) and ensemble spread (shaded) of simulations in Table 1 during 1850–2005 with a reference period of 850–1849, and (c) same as (b) but with a reference period of 1950–1979.  
 370

In the western region (Fig. 3a), ~~NOAH-LSM~~ NOAH-LSM-ERA5 is characterized by positive correlations at high latitudes over  $60^{\circ}\text{N}$  and negative correlations at the mid-latitudes, a pattern that resembles the NAO. CESM1 and CCSM4 show to some extent, the most similar correlation patterns to NOAH-LSM. GISS-E2-R and MIROC-ESM exhibit similar positive  
 375

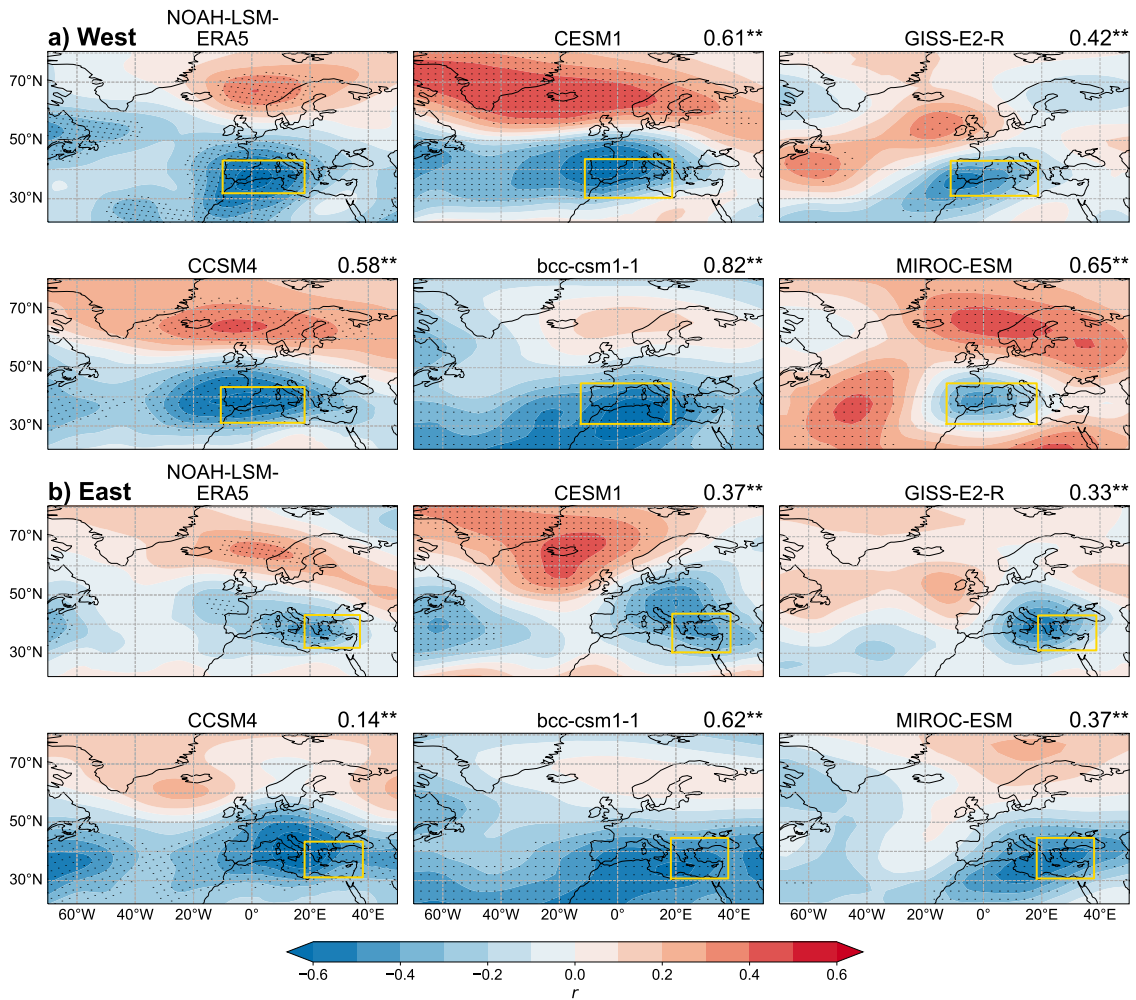


**Figure 3.** Pearson correlation coefficients ( $r$ ) between the time series of Z500 and SOIL in for (a) the western and/or (b) the eastern Mediterranean and Z500. The dots highlight For the climate models — CESM1, GISS-E2-R, CCSM4, bcc-csm1-1, and MIROC-ESM — the first ensemble member is used for the calculation. The dotted regions highlight where the correlations are statistically significant at the 5% level. Yellow squares indicate (a) the western and (b) eastern Mediterranean regions where the area-weighted spatially-weighted soil anomalies (SOIL) are calculated/obtained. Note that the yellow squares delimiting each region differ slightly between the models since the horizontal resolutions are not interpolated to the same grid. The numbers on the top left of the panels indicate the  $r$  between the correlation patterns of NOAH-LSM-ERA5 and the corresponding climate model. The number is denoted with \*\* when it is statistically significant at 95% confidence level.

correlations over the high latitudes, but the spatial extent and location differ from those in NOAH-LSM/NOAH-LSM-ERA5. The bcc-csm1-1 does not present any statistically significant correlations north to over 50°N.

In the eastern region (Fig. 3b), ~~NOAH-LSM-NOAH-LSM-ERA5~~ shows negative correlations over southern Europe, and positive correlations are ~~found~~ located at high latitudes over the Scandinavian Peninsula. This pattern is similar to that for the western Mediterranean, but with lower values and a slightly different spatial extent. CESM1 exhibits the most similar pattern to the ~~NOAH-LSM-NOAH-LSM-ERA5~~. The rest of the models also show negative correlations over southern Europe, ~~but the correlations outside of Europe are not significant~~. For GISS-E2-R and MIROC-ESM, the correlations are mostly significant in the European domain but not outside of the continent.

The numbers on the top of the panels indicate the correlation between the correlation patterns of NOAH-LSM-ERA5 and each of the climate models presented in Fig. 3. The correlation analysis is performed on the entire regions in Fig. 3, which means that these values measure the overall closeness of the entire correlation fields to NOAH-LSM-ERA5 without considering the statistical significance of individual grid locations. We use this quantity to compare the model's representation of SOIL-related Z500 patterns between the two regions, the western and eastern Mediterranean. Overall, the correlation coefficients are higher in the western region than in the eastern Mediterranean. In the western region, the maximum coefficient is 0.82, shown by bcc-csm1-1, while the maximum in the eastern region is 0.62, also by the same model. The minimum value in the western region is 0.42 by GISS-E2-R, and in the eastern region, it is 0.14 by CCSM4. The overall comparison of spatial correlation coefficients implies that the variability of Z500 associated with SOIL in the climate models is better represented over the western region than over the eastern region.

Nevertheless, all models present similarities to the ~~NOAH-LSM-NOAH-LSM-ERA5~~, fed with the present observational data, exhibiting a center of negative correlations in southern Europe with larger values over the focus regions. In general, CESM1 resembles the ~~NOAH-LSM-NOAH-LSM-ERA5~~ in both target regions better than the other models, although some difference exists in the spatial extent of significant correlations. The difference in correlation patterns between the models can be due to the model-dependent internal ~~variability~~, climate dynamics and a relatively shorter time period (56 years) considered for the correlation analysis. A time series of 56 years may not include all possible variability of SOIL and Z500, and could also influence the significance level of the statistical tests. A potential implication of the difference between the models on the analysis is discussed again in the coming sections.

#### 4.2 Mediterranean drought characteristics during the last millennium (850–2005 CE)

Before examining droughts for the entire last millennium in the climate simulations, it is necessary to ~~reexamine~~ remark that the drought definition is sensitive to the reference period. For instance, when 850–1849 CE (LM) is ~~selected~~ considered as the reference period to calculate the soil moisture anomalies, the Mediterranean region is under a constant long-term dry condition during the entire historical period (~~Fig. 2b~~). ~~The continuous negative SOIL in Fig. 2b indicates figure not shown~~. This means that the mean climate was wetter in LM than in the upcoming following decades, a change that is mostly attributed to anthropogenic effects on global and regional climate (~~Masson-Delmotte et al., 2021~~). ~~Although the magnitude of the negative trend is the same, it is noticeable that these~~ (Douville et al., 2021; Seneviratne et al., 2021). These continuous negative SOIL conditions are not apparent when the recent period (1950–1979) is considered for the anomaly calculation (Fig. 2a). ~~To~~



Therefore, to analyze the entire ~~Common Era together last millennium continuously~~ without the influence of the recent anthropogenic forcing, ~~the ensemble means of SOIL are extracted from each ensemble member~~ each model's ensemble mean of SOIL is extracted from the corresponding model's ensemble members of Hist (Fig. 2c) as explained in Section 3.1. The time series of the number of drought years ~~in a moving window of a century for each model and region (per century) for 850–2005 CE~~ are presented in Fig. 4. In addition, the percentage of total drought years and the mean duration of ~~the~~ droughts are included.

The number of total drought years and the mean duration vary across the models. Compared to the other models, MIROC-ESM shows a reduced percentage of total drought years in both regions (7.02% for the western region and 7.63% for the eastern region). The percentages of droughts in the other models range from 9.26% (GISS-E2-R) to 11.24% (CCSM4) for the west, and from 8.77% (GISS-E2-R) to 11.44% (bcc-csm1-1) for the east. The mean duration varies from 4.07 years (CCSM4) to 4.62 years (bcc-csm1-1) for the west, and 3.95 years (CESM1) to 4.71 years (MIROC-ESM) for the east. For the duration, unlike for the total drought years, MIROC-ESM shows comparable duration to other models and higher values than others in the east, indicating that in MIROC-ESM, there are fewer droughts but with longer duration.

The time series of drought years (Fig. 4) show that no simultaneous period of increasing or decreasing drought events is observed ~~between across~~ the models. For ~~example, an apparent decrease instance, the apparent decreases~~ in drought events in 1600–1650 CE in GISS-E2-R ~~does in the east and during mid-1500 CE in CCSM4 do~~ not appear in any of the other models. ~~The same happens for the no-drought period in the eastern Mediterranean Increased drought events in the west during mid-1500 CE are only shown in CCSM4. In addition, in CESM1 and GISS-E2-R, which are the two models that have more ensemble members during LM, there is large variability in drought occurrence. The same is also observed across the ensemble members of the same model, not showing a common period with similar drought occurrence in LM. This fact emphasizes that external forcing signals do not play a role in droughts over the Mediterranean, indicating that internal variability. The ensemble members of CESM1 and GISS-E2-R do not exhibit unanimous periods of low or high drought occurrence (figure not shown). This large variability in drought occurrence across the models and the ensemble members, depicted by the ensemble spreads in Figs. 4 and 2b, implies that internal climate dynamics is the primary driver of droughts in the region during LM and a counterfactual Hist without anthropogenic forcing. Hist with the anthropogenic forcing removed. In these time series, external or volcanic forcing signals are not visible in the variability of droughts.~~ More precisely, although external forcing can affect drought occurrence, their influences are masked by internal ~~variability~~ climate dynamics. This observation is in line with previous climate model-based studies (Xoplaki et al., 2018; Kim and Raible, 2021) and proxy-based studies (Cook et al., 2016; Rao et al., 2017). Volcanic eruptions which strongly affect the global hydroclimate on a multi-year time scale are ~~more known to be related to wetter conditions over the Mediterranean (Iles and Hegerl, 2014; Rao et al., 2017; Kim and Raible, 2021). Although external forcing (Iles and Hegerl, 2014; Gao and Gao, 2017; Kim and Raible, 2021). Although other external forcings could be associated with a much longer fluctuation of dryness and wetness over the region (e.g., millennial to orbital scales; Stockhecke et al., 2016), these time scales are beyond the scope of this study.~~

In the ~~simulations~~ number of drought years in Fig. 4, an anti-phase of drought occurrence with multi-decadal time scales ~~is observed~~ between the western and the eastern regions ~~is observed~~, more clearly in those models and periods with one ensemble member. This anti-phase ~~is seems to be~~ in line with Roberts et al. (2012) ~~and can be associated with dominant drought driving~~

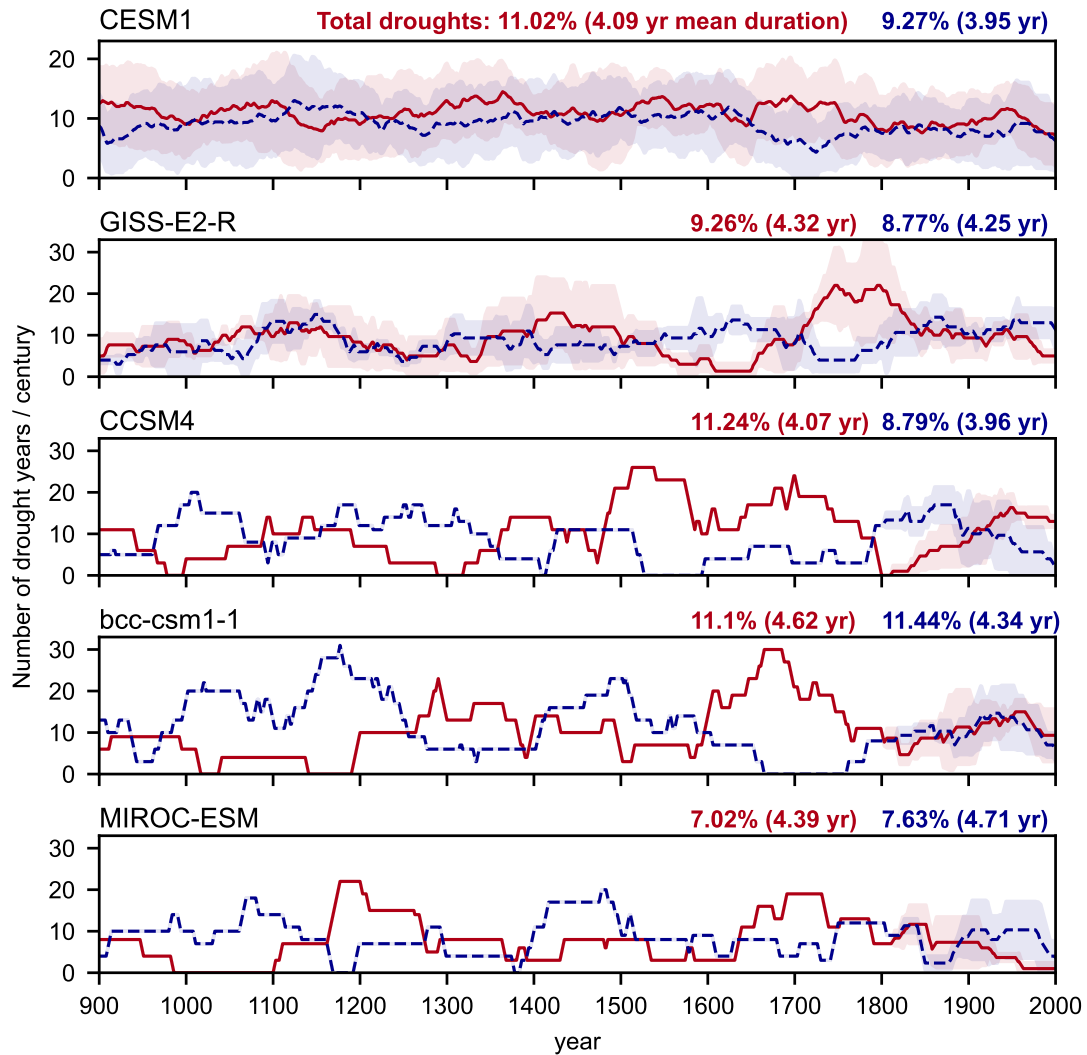


**Figure 4.** Occurrence-Number of drought years in a moving window of a century in the western (red) and eastern Mediterranean (blue). Thick lines for those models and periods that have more than one ensemble member correspond to the ensemble mean, and color-shading indicates the ensemble spread represented by a unit standard deviation. The mean percentages of total drought years and the mean duration of droughts are calculated from the ensemble means, and they appear in the top-right part of each panel. Ensemble spreads of occurrence are shaded. Note that the y-axis in CESM1 (first panel) is different from others.

circulation patterns of each region. More details on this are provided in the next sections. For. At the same time, for some periods, simultaneous drought occurrence between-in both the western and eastern regions is detected in both regions, for instance, 1100-1150 CE in CCSM4 and 1400-1450 CE in bcc-csm1-1, which. This seems to agree with Cook et al. (2016). However, this-

450 To evaluate closely the dominant frequency of the association between the two regions, and their temporal co-variability, the wavelet coherence analysis is performed on the time series of SOIL (Fig. 2b) and presented in Fig. 5a. At first glance, the wavelet coherence analysis suggests that timing and frequencies of co-variability are not the same across the models for both the soil moisture anomalies and the number of droughts. Also, the association is not uniform across the time-frequency space. The analysis performed on SOIL between the western and eastern regions (Fig. 5a) indicates co-variability that ranges from  
455 interannual to multi-decadal time scales, depending on the model. CCSM4 shows co-variability of higher frequencies (less than a 32-year period.). In general, the association between the two regions is in-phase~~variability does not occur as noticeably as the anti-phase relationship in the model simulations. For those models and periods with more ensemble members, the ensemble means also exhibit this.~~The co-variability between the western and eastern regions from all models is less pronounced and less significant in all time-frequency bands compared to the result presented by Cook et al. (2016) based on OWDA, which has  
460 shown significant in-phase co-variability of SOIL between east and west in diverse timescales.

The time series of SOIL does not necessarily indicate that dry periods are in phase. To compare only the dry periods, the wavelet coherence analysis is performed on the number of drought years (Fig. 4), which is presented in Fig. 5b. The co-variability between the two regions is significant in some time scales, for instance, on a multi-decadal time scale (around 32 years and higher) with an anti-phase~~relationship between the west and east, although sometimes this association~~relationship  
465 in CESM1, bcc-csm1-1, and MIROC-ESM. For GISS-E2-R, CCSM4, and MIROC-ESM, the anti-phase association is also significant on a high-frequency band (of less than 32 years). This result seems to agree with the observation from Fig. 4. It is observed that the anti-phase co-variability also depends on the time period, for instance, CCSM4 during 1400-1500 CE, the co-variability is~~blurred by the ensemble spread. During Hist (Fig~~in-phase. Again, the overall result points out the associations that are not uniform across time and that vary across the models. The occurrence of droughts and dry periods can be associated  
470 with dominant drought-driving circulation patterns of each region. More details on this are provided in the next sections.~~2b) the entire Mediterranean shows concomitant dryness reflecting the dominance of anthropogenic influence over the natural variability.~~

### 4.3 Circulation patterns associated with droughts

The PC-KCA-PCC method (Section 3.5) is used to detect drought-related circulation patterns in Z500 of the climate sim-  
475 ulations. In total, 11 drought-associated~~pattern groups~~circulation patterns are detected. These ~~pattern groups~~patterns are presented in Fig. 6, with their frequencies (in the number of occurrences per century) during 850–2005 CE. Each pattern group is a mean of a certain number of clusters. The first five ~~pattern groups~~patterns contain 83% of the entire drought years (Fig. 6). The list of models and experiments included in each pattern group are included in Table A1.

Some pattern groups resemble the well-known modes of climate variability: P1 is the combination of a high-pressure sys-  
480 tem over Europe and a positive NAO pattern. This circulation pattern is similar to those observed in the correlation composite duringthe present day in the western Mediterranean (Fig. 3a), and it is commonly associated with Mediterranean droughts (Xoplaki et al., 2018; Kim and Raible, 2021). P2 is a negative NAO pattern with a center of negative anomalies in the mid-latitudes extending from the Atlantic Ocean to Europe. P3 is the opposite phase of P2, whichalso resembles a

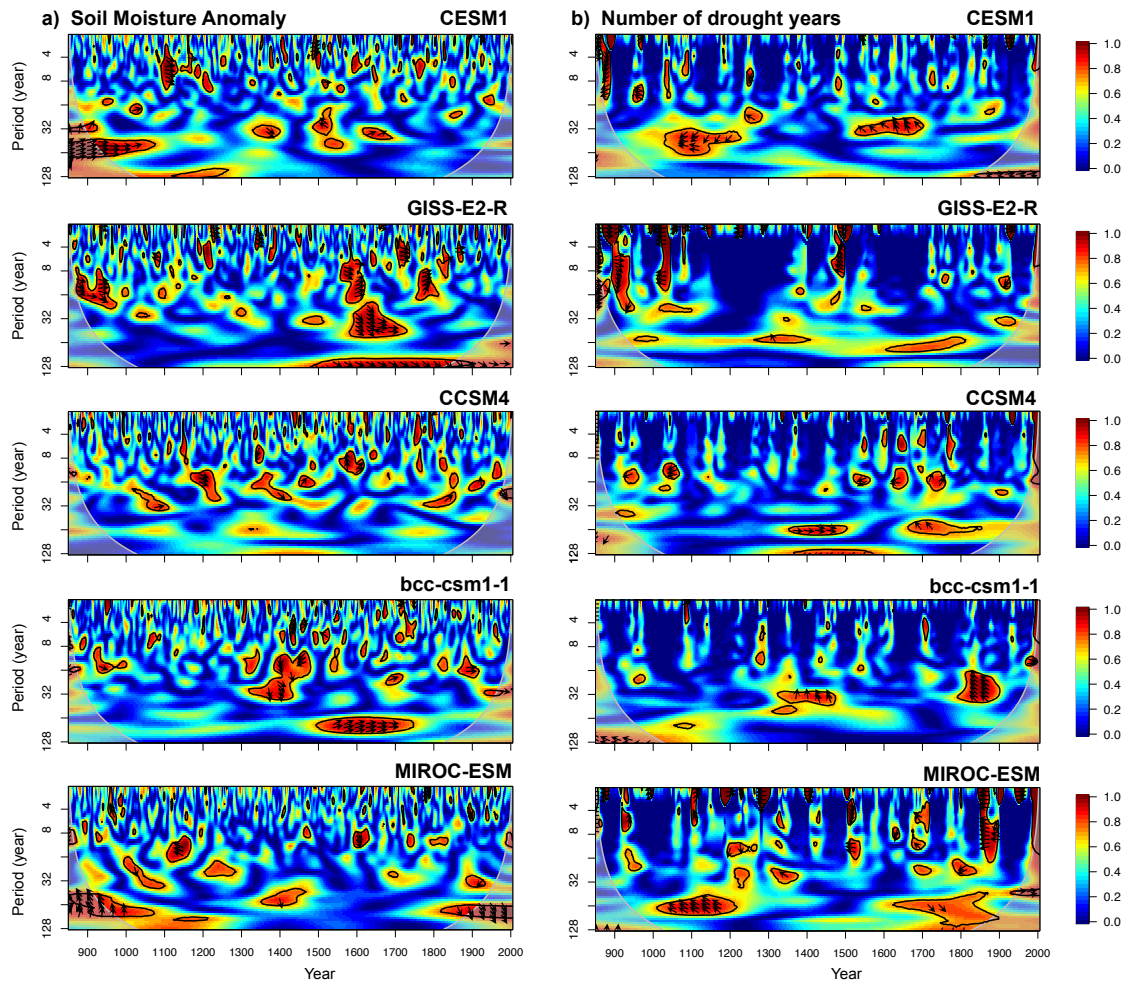


**Figure 5.** Wavelet coherence analysis between the western and eastern Mediterranean for the time series of (a) SOIL and (b) 100-year moving number of drought years, depicted in the time–frequency space. For those models and experiments with more than one ensemble member, the analysis using only the first member is shown. For (a), SOIL in the west is obtained over a smaller area domain  $10^{\circ}\text{W}–0^{\circ}$ ,  $32^{\circ}–42^{\circ}\text{N}$ , mostly encompassing the Iberian Peninsula northern Morocco, to make it consistent with Cook et al. (2016). The red-shaded regions indicate where the co-variability between the western and eastern regions are statistically significant at 95% confidence level, estimated from Monte Carlo resampling of the time series. The arrows indicate the phase relationship: to the right (left) when the two time series are in-phase (anti-phase), and to the up (down) when the first (second) time series is the leading one.

485 positive NAO. These three patterns enclose 62% of the total occurrence, highlighting the importance of the NAO for Mediterranean droughts. Positive NAO is known to be the dominant climate mode that drives a drier condition over the Mediterranean region (Lionello et al., 2006; Kim and Raible, 2021). This explains a large percentage of occurrence of P1 and P3 (42%) during droughts. Although it seems contradictory that P2 depicting a negative NAO condition also occupies a significant percentage of

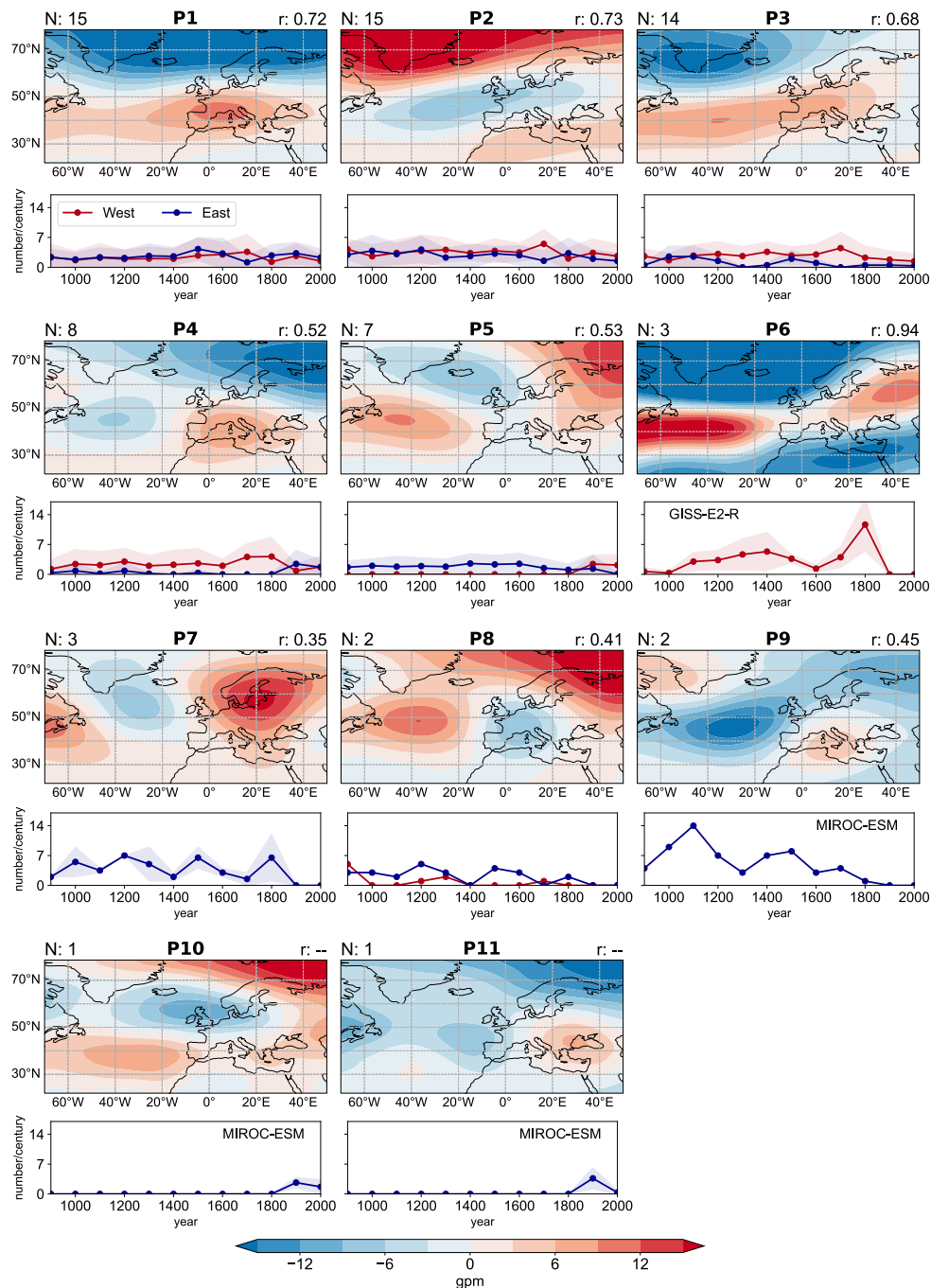


**Figure 6.** Z500 anomalies that represent the extratropical circulation patterns from P1 to P11 associated with Mediterranean droughts. The number of clusters N averaged to make these mean circulation patterns are presented on the top-left part of each map. The mean Pearson correlation r between the clusters within each circulation pattern appears on the top-right part. Below each map, the time series of the number of occurrences of the corresponding patterns per century for the western (red) and eastern (blue) Mediterranean are plotted, together with the respective ensemble spread of occurrence (shaded). When only one climate model belongs to a circulation pattern P, its name appears on the panel.

the occurrence (20%), the occurrence of P2 indicates the fluctuation of NAO patterns throughout multi-year droughts. P4 shows a similar high-pressure system over central and southern Europe, but with negative Z500 anomalies in the Atlantic Ocean and high latitudes. P8 seems to be the opposite phase of P4. It is a wave-train pattern extending over the northern Atlantic and Europe, resembling an EA-WR pattern. P5 is similar to the Eastern Atlantic pattern.

Besides the patterns that are comparable to the well-known modes of variability in the mid-latitudes, some patterns exhibit more unique characteristics and are derived from one model only. The spatial structure of P6 with positive Z500 in the mid-latitudes and negative Z500 in the high latitudes is similar to a positive NAO in P3, but with a distinctly different Z500 anomaly over land. This pattern only appears in GISS-E2-R. P10, characterized by positive anomalies in the Atlantic and negative anomalies in central and northern Europe, and P9 and P11, with a high-pressure system centered over the eastern Mediterranean, are all derived from MIROC-ESM.

~~Extratropical pattern groups P1 to P11 associated with Mediterranean droughts, in which temperature anomalies are shaded and the contour lines show the associated Z500 field. Negative and positive Z500 values are plotted with dashed and solid lines, respectively. The number of clusters  $N$  is included on the top-left part of each map, while the mean Pearson correlation between the clusters in each pattern group  $r$  appears on the top-right part. Below each map, the time series of occurrence of droughts per century for the western (red) and eastern (blue) Mediterranean are plotted, together with the respective ensemble spread of occurrence (shaded). When only one climate model belongs to a group pattern  $P$ , its name appears on the panel.~~

~~In terms of surface temperature anomalies, regions with high pressure anomalies exhibit positive temperature anomalies. Although in general, temperature conditions are not the main driver of the initiation of droughts, they can be a factor that contribute to the continuity of droughts when warm conditions occur over the target region (western or eastern Mediterranean) (Kim and Raible, 2021).~~

The frequencies of occurrence occurrences of the patterns (panels below each map in Fig. 6) indicate that droughts are associated with different circulation patterns. However, some ~~pattern groups~~ patterns occur more frequently than others and are apparent only in some periods. The western and eastern Mediterranean do not always share the same patterns. P1 (high-pressure system and positive NAO-like) and P2 (negative NAO-like) appear in both regions with a similar frequency over time. P3 (positive NAO-like) and P4 (high-pressure system in central and southern Europe) occur more frequently in the western region, and P6 from GISS-E2-R is only associated with droughts over the western Mediterranean. P5 (EA-like) and P8 (low-pressure system in Europe) are more apparent in the east. P7 (EA-WR-like), P9 and P11 (high-pressure system in the east), and P8 are only associated with droughts over the eastern Mediterranean. Note that the last three pattern groups are from MIROC-ESM.

~~Mean occurrence of drought-associated pattern groups during the last millennium (LM) and historical (Hist) periods for each climate model over the (a) western and (b) eastern Mediterranean. Similar patterns in spatial Z500 anomalies are coloured with the same colour, but with different patterns. The black vertical lines indicate the spread of occurrence. The frequencies of occurrences of the patterns presented in the lower panels of Fig. 6 indicate that the occurrence is not uniform over time, with certain patterns appearing only during specific periods. Nevertheless, the dominant frequency of each circulation pattern is estimated using a power spectra analysis (i.e., Cook et al., 2016), and the result reveals that the values noticeably vary across~~

the models (Fig. A2). In general, the most dominant frequencies span a wide range of the multi-decadal (10-100 years) time scales, which partially seems to explain the time scales of the co-variability of SOIL and drought periods in Fig. 5.

525 Fig. 7 shows the mean occurrence of pattern groups for each model during summarizes the mean frequencies of the circulation patterns during the entire LM and Hist ~~Extended~~ in Fig. 6, represented by the mean number of patterns per century for each model. An extended version of Fig. 7 can be found in Fig. A1, which shows the time series of ~~occurrence of pattern groups~~ the number of occurrences of the patterns for each climate model. For simplicity, in Fig. 7, the patterns are classified by their similarity in spatial Z500 anomalies. For instance, those with high pressure over central Europe or the Atlantic Ocean and a positive NAO-like are shaded in red (positive-type pattern). The same is for the patterns characterized by the low-pressure system and/or negative anomalies and a negative NAO-like over the same region ~~but~~ in blue (negative-type pattern). 530 Fig. 7 indicates that the positive- and negative-type patterns are shared by all models. As shown by Fig. 4, the frequencies of these patterns vary across the model and time period. In addition, some patterns are more noticeable in some models than others. The EA-WR-like pattern appears in CCSM4 and bcc-csm1-1 but not in CESM1, GISS-E2-R, and MIROC-ESM. Some patterns occur dominantly during one period. For example, P6, P7, and P9 are patterns that are visible during LM. However, P10 and P11 in the eastern and P5 over the western region appear only during Hist. In addition, the ensemble spread of pattern occurrence (black bars in Fig. 7) is also an important quantity to consider as it shows large variability in the occurrence of a pattern during the same period. 535

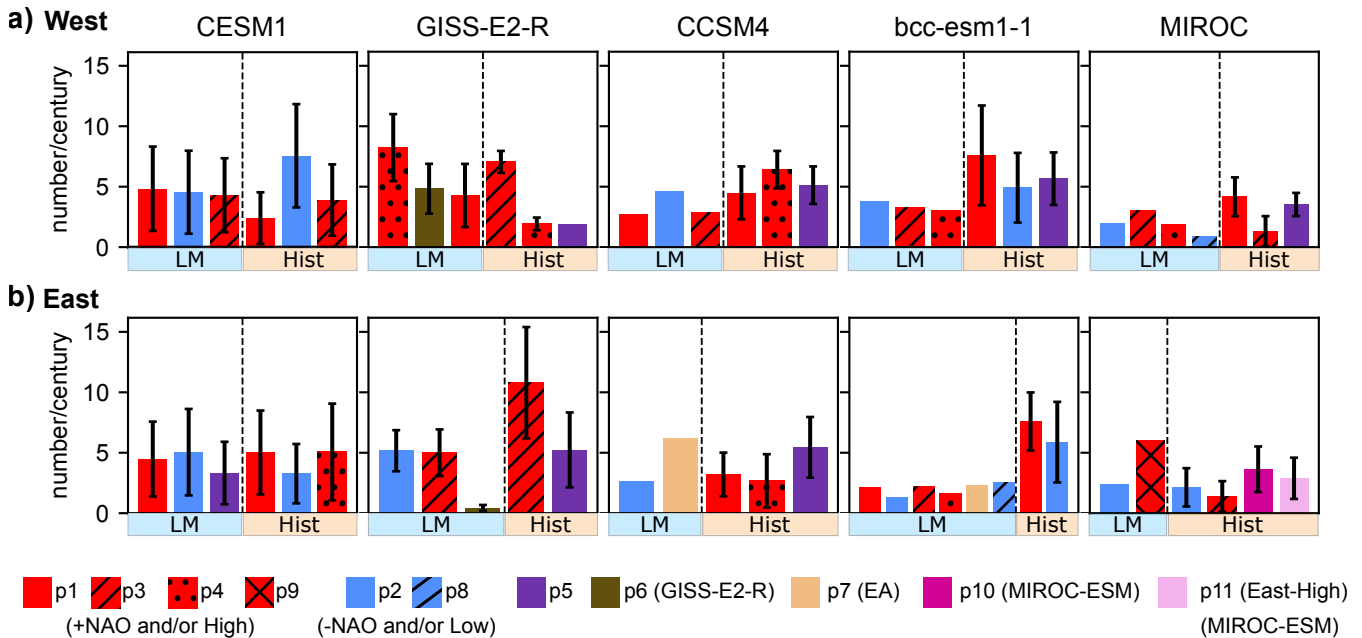


**Figure 7.** Mean occurrence of drought-associated pattern groups during the last millennium (LM) and historical (Hist) periods for climate model over western and eastern Mediterranean. Similar patterns in spatial Z500 anomalies are plotted colored with the same color but with different patterns. The black vertical lines indicate the spread of occurrence.

## 5 Discussion

540 It is arguable that the detected ~~pattern-groups~~ drought-associated circulation patterns and their frequencies depend on the numbers of  $N$  PCs and  $k$  clusters used for the method. We only take some PCs and clusters that explain an acceptable percentage of variance to increase the robustness of the clustering method. This approach may exclude certain Z500 anomalies that are outside the threshold. However, the percentage of variance in the same period is not distinctly different between the models (Table 2). They are between 72% to 78% in LM (around 80% in Hist) and with  $k = 3$  in most of the models (maximum 6 or 7  
545 for a few models). Hence, it is possible that the method may be sensitive to the selected parameters, and it may exclude some variability with a low occurrence, but it does not affect the comparability between the models.

Another finding is the difference in the detected patterns between LM and Hist. Some patterns appear only in one period and not in another. This difference in LM and Hist may occur because Z500 of each ~~period are included separately in experiment~~ is fed separately into the clustering method (Section 3.5), and the Hist simulations cover a much shorter period than LM. Some  
550 patterns may not occur frequently during this short period. Taking out an ensemble mean from the ensemble members may also influence the spatial patterns of Hist, as the values of ensemble means can be sensitive to the number of simulations (Maher et al., 2018). However, any statistical detrending method to exclude the recent anthropogenic forcing contains similar statistical drawbacks. For instance, the trend during Hist is not uniform over the entire period ~~and~~, that could cause some difficulties ~~to~~  
~~select in selecting~~ a suitable detrending period in a linear or polynomial detrending method.

555 It needs to be pointed out that MIROC-ESM presents many unique patterns that fail to join other ~~pattern-groups~~ circulation patterns, largely occurring with the eastern Mediterranean patterns. ~~We assume that this can be related to the horizontal and vertical resolution of land grid points in MIROC-ESM.~~ Several reasons can be put forth to explain this particular characteristic of MIROC-ESM. As depicted in Fig. 2, MIROC-ESM presents a different SOIL trend compared to the other models during Hist. This distinct trend could potentially be attributed to different circulation types compared to those of other models.

560 Another argument to consider is that, in general, SOIL-related circulation fields in the eastern region seem to exhibit lower statistical similarity with the observation-based circulation condition, based on correlation coefficients in Fig. 3b. While this is the case for all models, lower correlation coefficients in the eastern regions can be associated with a reduced number of horizontal grid points compared to the western regions. Fewer grid points may not reflect the entire temporal variability of SOIL, and, therefore, the associated circulation variability.

565 Particularly, MIROC-ESM has only half of the grids compared to bcc-csm1-1 over both the western and eastern regions and presents relatively coarse vertical soil layers (Table 1). The coarse ~~vertical and horizontal resolutions of land grid points~~ horizontal resolutions over the land and atmosphere may affect the variables associated with soil moisture, such as precipitation, which is sensitive to the horizontal grid size (Haren et al., 2015). ~~Moreover, scarce land grid points and vertical levels. In addition, poor land vertical resolutions~~ are probably insufficient to represent ~~land hydrology and the processes associated with~~  
570 precipitation (Champion et al., 2011). This soil hydrology associated with vegetation and soil moisture memory effects that affect regional hydroclimate conditions (Hagemann and Stacke, 2015). This also can be the reason why MIROC-ESM shows spatial correlation patterns that differs distinctly from NOAA-LSM outside the focus region (in Fig. 3).



575 Assessing which model represents soil moisture variability, therefore also its related circulation, better is a complicated task since it is known that the magnitudes of soil moisture depend largely on the internal physics of land surface models (Fang et al., 2016; Berg and Sheffield, 2018). Moreover, soil moisture interactions with the atmosphere (Berg and Sheffield, 2018) and vegetation dynamics related to soil processes (Huang et al., 2004) vary across the CMIP5 models. Choosing the same vertical soil moisture level (70 cm) across all the models to represent ecosystem-related depth, i.e., root zone, over the entire Mediterranean region may be another influential factor since the root zone varies with the region (Kleidon, 2004).

580 As here the objective is not to choose the best or worst model but to examine differences among the climate models, we use the same threshold for the soil moisture for all models. By setting the same criterion, we can better distinguish the differences among the PMIP3-CESM1 models in droughts and related circulation and also relate them to the models' vertical and horizontal spatial resolutions.

Regarding the pattern groups, in all models, NAO-like and high pressure and ridge over central Europe occur more frequently in the western Mediterranean droughts. The influence of positive NAO is weaker over the eastern region, presenting a lower frequency of occurrences. The eastern region is more dominated by eastern-type patterns, such as an EA-like pattern or eastern-centered high, where the center of positive Z500 anomalies is located over the eastern Mediterranean and weak or negative Z500 anomalies are found over the western region. These findings agree with already known studies on present observation-based dry periods (Xoplaki et al., 2004, 2012). The link between the NAO and EA patterns and Mediterranean droughts is also identified in a tree-ring-based reconstruction study by Cook et al. (2016) and Markonis et al. (2018). Different to the proxy-based studies, our study shows that the EA influence is largely concentrated in the eastern region.

The detected circulation patterns explain to some extent the anti-phase drought occurrence between the western and eastern Mediterranean in Fig. 4. In general, patterns involved in droughts in one region are characterized by strong positive Z500 in the focus region but by weak anomalies in another region. Such Z500 anomalies would bring dryness and warm conditions to the focus region and a relatively less dry condition to another region, agreeing with Dünkeloh and Jacobeit (2003); Roberts et al. (2012). If these patterns are able to persist longer in time over a target region, that is, occurring more frequently during a certain period, then the other region may experience a long-lasting opposite condition. However, the mechanisms that maintain these interannual patterns to persist longer or to occur more frequently, contributing to a multi-decadal scale anti-phase relationship, still remain elusive. ~~Our This~~ result showing the anti-phase drought occurrence between the west and east ~~supports seems to be in line with~~ the lake sediment-based reconstruction by Roberts et al. (2012) ~~but is in contrast to the tree ring-based reconstruction by Cook et al. (2016). This difference between.~~ However, in the models, the periods of the anti-phase co-variability of droughts periods, also in-phase co-variability of soil moisture anomalies in Fig. 5 are not uniform across the time periods, and the dominant time scales also vary across the models. This indicates a clear difference between the models and proxy-based reconstruction may possibly be explained by large discrepancies in different hydroclimate reconstructions and different intrinsic characteristics of each proxy (Cook et al., 2016). records.

605 Our analysis also shows that the contribution of the patterns to droughts may greatly depend on the choice of the model. For example, the importance of EA-WR in the eastern droughts is apparent in CCSM4 and bcc-csm1-1 but not in other models

(Fig. 7). The frequencies of a shared pattern between some models also vary greatly among them. This highlights the fact that climate models have their preferred circulation patterns associated with Mediterranean droughts.

## 6 Conclusions

610 We identify circulation patterns in the Euro-Atlantic domain associated with persistent droughts in the western and eastern Mediterranean regions during 850–2005 CE in several CMIP5-PMIP3 and CESM-LME climate simulations and perform comparisons across these climate models. Droughts are quantified through annual anomalies of vertically integrated 70 cm soil moisture and circulation patterns through the annual anomalies of geopotential height at 500 hPa.

Our findings emphasize that Mediterranean droughts are ~~driven by internal variability~~ related to circulation patterns from internal climate dynamics, which is in line with previous studies (~~e.g., Cook et al., 2016; Xoplaki et al., 2018~~) (e.g., Cook et al., 2016; Xoplaki et al., 2018). Extratropical circulation patterns associated with Mediterranean droughts resemble the major climate patterns in the Euro-Atlantic region: western Mediterranean droughts are dominated by a high-pressure system over central Europe and an NAO-like pattern, while eastern Mediterranean droughts are linked to positive pressure anomalies in the southern and eastern Mediterranean, negative NAO, EA and EA-WR like patterns. ~~An~~ For some periods, an anti-phase of drought ~~variability periods~~ between the west and east is found in this study, which agrees with Roberts et al. (2012) and Dubrovský et al. (2014). The circulation patterns ~~also~~ and their frequencies seem to explain the anti-phase ~~behaviour in the western versus~~ behavior between the western and the eastern Mediterranean. ~~However, the~~ If one region experiences strong positive Z500, another region is characterized by weak anomalies during the same period. The mechanisms that drive the persistence of these patterns leading to a multi-decadal scale relationship remain elusive. ~~This anti-phase variability is not apparent when the GHG-forced signal is included from 1850. In this case, both the western and eastern Mediterranean show a coherent decrease in soil moisture anomalies. However, the periods of this co-variability of soil moisture anomalies and droughts periods are not temporarily synchronous across all the models and are significant only during some specific periods. This result of fewer significant periods and frequencies differs from the study by Cook et al. (2016) based on a proxy reconstruction during the growing season and indicates a clear difference between the models and proxy-based records.~~

630 Some circulation patterns associated with droughts occur more frequently than others, but not a single pattern dominates a certain region and period. Some patterns are only apparent in one model, indicating that the main drivers of droughts are different between the models. Moreover, large discrepancies in drought occurrence exist between the models and within the ensemble members of the models. This observation highlights model-dependent internal ~~variability~~ climate dynamics. Model differences in drought occurrence and patterns can ~~be also~~ also be attributed to the resolution of a model: ~~we noticed that~~ coarse horizontal and vertical resolutions of land grid points ~~may~~ might not reflect well the soil moisture variability and its associated circulation. For instance, MIROC-ESM shows distinct soil moisture variability and drought-related circulation patterns to other models. All these differences between the models can be a source of uncertainty that complicates model-proxy comparisons.

This work attempts to identify drought-associated extratropical circulations, focusing on natural climate variability ~~;~~ in each individual climate model and comparing these drought-related characteristics across the models. In this way, differences

640 between the models are identified better, including how they represent the baseline climate for droughts. Our results can also be helpful in understanding model discrepancies and uncertainties in future drought projections, for instance, to examine which drought-associated modes of climate variability are preferred by each model, and how these modes will change under different climate change conditions. A more detailed understanding of these differences may contribute to better future projections, hence, aid long-term preparedness for droughts over the region.

645 *Code and data availability.* The codes to reproduce the analysis performed in this manuscript will be available on GitHub upon acceptance of the manuscript. All the datasets used in this study are freely available online: CESM-LME at <https://www.earthsystemgrid.org/>, CMIP5 at <https://esgf-node.llnl.gov/projects/cmip5/>, ERA5 at <https://cds.climate.copernicus.eu/>, and NOAA-LSM soil moisture at [https://disc.gsfc.nasa.gov/datasets/GLDAS\\_NOAH025\\_3H\\_2.1/summary](https://disc.gsfc.nasa.gov/datasets/GLDAS_NOAH025_3H_2.1/summary).

*Author contributions.* WMK designed the study and conducted the analysis in discussion with CCR. WMK set up the methodology with the input of SJGR. WMK and SJGR prepared the first draft of the manuscript. All authors contributed to the scientific discussion and writing of the manuscript.

*Competing interests.* The authors declare that they have no conflict of interest.

*Acknowledgements.* We acknowledge the World Climate Research Programme's Working Group on Coupled Modelling, which is responsible for CMIP, and we thank the climate modeling groups (listed in Table 1 of this paper) for producing and making available their model output. For CMIP, the U.S. Department of Energy's Program for Climate Model Diagnosis and Intercomparison provides coordinating support and led development of software infrastructure in partnership with the Global Organization for Earth System Science Portals. We also acknowledge the Copernicus program for the ERA5 data (Hersbach et al., 2018) available in Copernicus Climate Change Service Climate Data Store, and the NASA/NOAA Global Land Data Assimilation System for the Noah Land Surface Model dataset (Rodell et al., 2004). WMK ~~acknowledge~~ acknowledges funding from the Swiss National Science Foundation (SNF; grant number P500PN\_206653). CCR is supported by the SNF (grant numbers 200020\_172745 and 200020\_200492) and Swiss National Supercomputing Centre (CSCS).

## Appendix A: Appendix

**Table A1.** Models and experiments pertaining to each pattern group after applying the PC-KCA-PCC method.

	<b>West</b>	<b>East</b>
<b>p1</b>	CESM1-LM, CESM1-H, GISS-E2-R-H, CCSM4-LM, CCSM4-H, bcc-csm1-1-H, MIROC-ESM-H	CESM1-LM, CESM1-H, CCSM4-H, bcc-csm1-1-LM, bcc-csm1-1-H
<b>p2</b>	CESM1-LM, CESM1-H, CCSM4-LM, bcc-csm1-1-LM, bcc-csm1-1-H, MIROC-ESM-LM	CESM1-LM, CESM1-H, GISS-E2-R-LM, CCSM4-LM, bcc-csm1-1-LM, bcc-csm1-1-H, MIROC-ESM-LM, MIROC-ESM-H
<b>p3</b>	CESM1-LM, CESM1-H, GISS-E2-R-H, CCSM4-LM, bcc-csm1-1-LM, MIROC-ESM-LM, MIROC-ESM-H	GISS-E2-R-LM, GISS-E2-R-H, bcc-csm1-1-LM, GISS-E2-R-H, MIROC-ESM-H,
<b>p4</b>	GISS-E2-R-LM, GISS-E2-R-H, CCSM4-H, bcc-csm1-1-LM, MIROC-ESM-LM	CESM1-H, CCSM4-H, bcc-csm1-1-LM
<b>p5</b>	GISS-E2-R-H, bcc-csm1-1-H, CCSM4-H, MIROC-ESM-H	CESM1-LM, CCSM4-H, GISS-E2-R-H
<b>p6</b>	GISS-E2-R-LM	
<b>p7</b>		CCSM4-LM, bcc-csm1-1-LM
<b>p8</b>	MIROC-ESM-LM	bcc-csm1-1-LM
<b>p9</b>		MIROC-ESM-LM
<b>p10</b>		MIROC-ESM-H
<b>p11</b>		MIROC-ESM-H

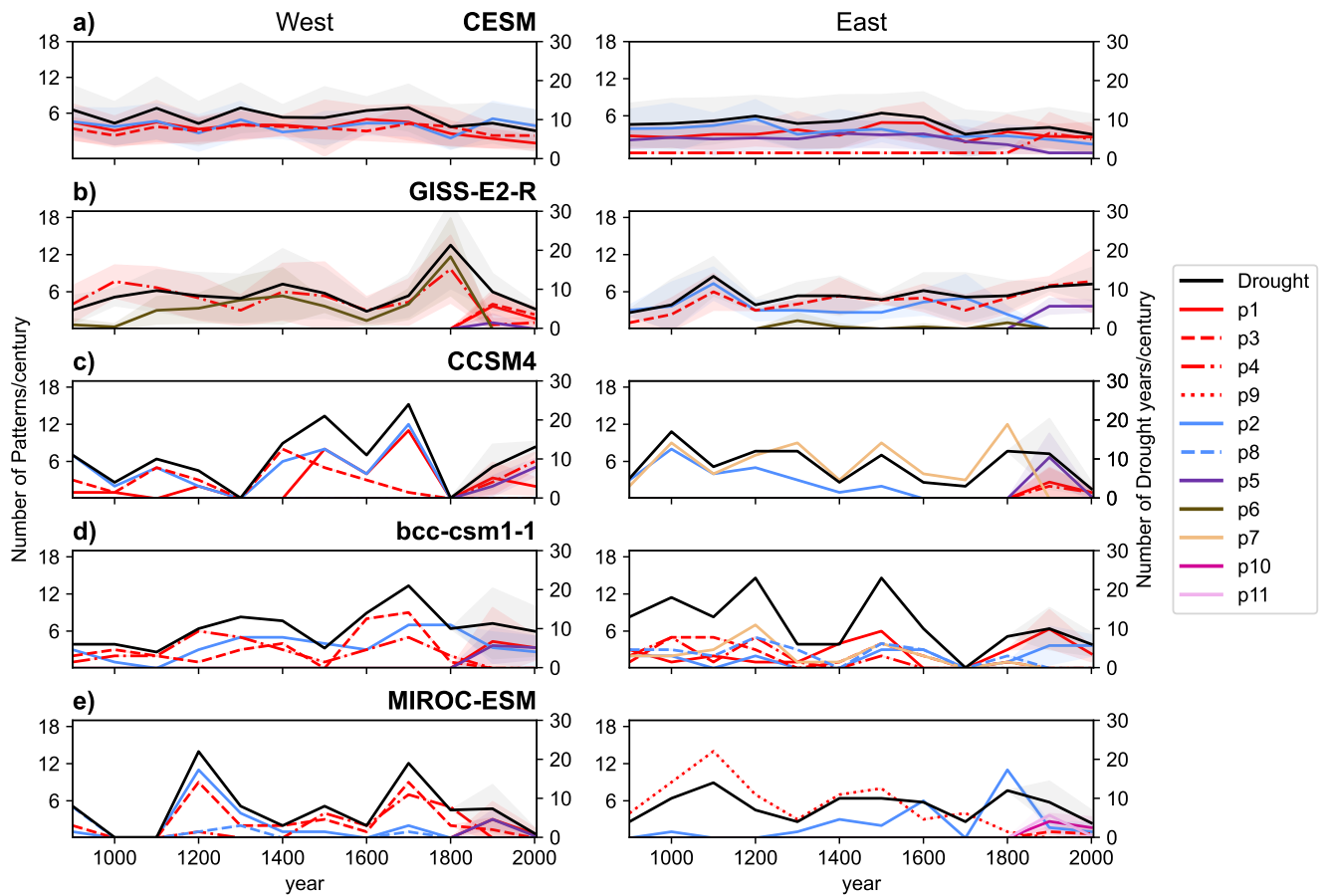


**Figure A1.** Extended version of Fig. 7: occurrence of each pattern group every century for each climate model.

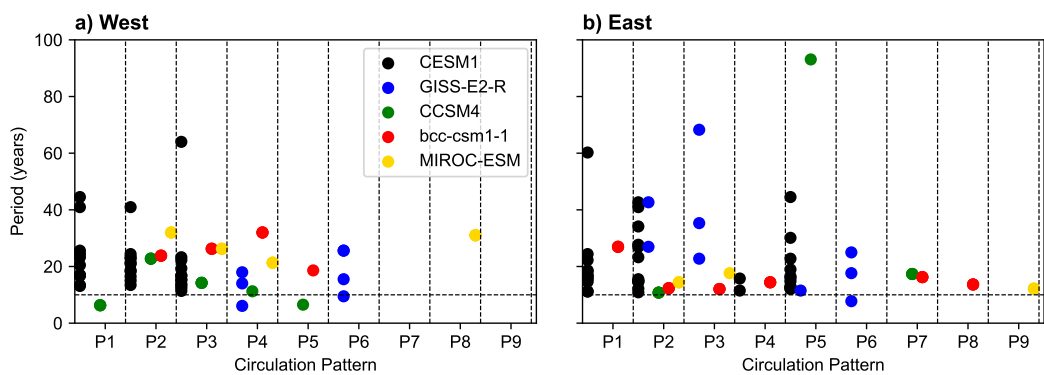


**Figure A2.** The most dominant frequencies (cycles/year) within the range of 0–100 year period from the power spectral density analysis (multitaper method with three tapers) applied to (a) western and (b) eastern mean SOIL during LM. Each dot indicates a value from one ensemble member.

## References

- Baek, S. H., Smerdon, J. E., Coats, S., Williams, A. P., Cook, B. I., Cook, E. R., and Seager, R.: Precipitation, Temperature, and Teleconnection Signals across the Combined North American, Monsoon Asia, and Old World Drought Atlases, *Journal of Climate*, 30, 7141–7155, 665 <https://doi.org/10.1175/JCLI-D-16-0766.1>, 2017.
- Berg, A. and Sheffield, J.: Soil Moisture–Evapotranspiration Coupling in CMIP5 Models: Relationship with Simulated Climate and Projections, *Journal of Climate*, 31, 4865–4878, <https://doi.org/10.1175/JCLI-D-17-0757.1>, 2018.
- Champion, A. J., Hodges, K. I., Bengtsson, L. O., Keenlyside, N. S., and Esch, M.: Impact of increasing resolution and a warmer climate on extreme weather from Northern Hemisphere extratropical cyclones, *Tellus A: Dynamic meteorology and oceanography*, 63, 893–906, 670 <https://doi.org/10.1111/j.1600-0870.2011.00538.x>, 2011.
- Coats, S., Smerdon, J. E., Seager, R., Cook, B. I., and González-Rouco, J. F.: Megadroughts in southwestern North America in ECHO-G millennial simulations and their comparison to proxy drought reconstructions, *Journal of climate*, 26, 7635–7649, <https://doi.org/10.1175/JCLI-D-12-00603.1>, 2013.
- Cook, B. I., Anchukaitis, K. J., Touchan, R., Meko, D. M., and Cook, E. R.: Spatiotemporal drought variability in the Mediterranean over 675 the last 900 years, *Journal of Geophysical Research: Atmospheres*, 121, 2060–2074, <https://doi.org/10.1002/2015JD023929>, 2016.
- Cook, E. R., Seager, R., Kushnir, Y., Briffa, K. R., Büntgen, U., Frank, D., Krusic, P. J., Tegel, W., Schrier, G. v. d., Andreu-Hayles, L., Baillie, M., Baittinger, C., Bleicher, N., Bonde, N., Brown, D., Carrer, M., Cooper, R., Čufar, K., Dittmar, C., Esper, J., Griggs, C., Gunnarson, B., Günther, B., Gutierrez, E., Haneca, K., Helama, S., Herzig, F., Heussner, K.-U., Hofmann, J., Janda, P., Kontic, R., Köse, N., Kyncl, T., Levanič, T., Linderholm, H., Manning, S., Melvin, T. M., Miles, D., Neuwirth, B., Nicolussi, K., Nola, P., Panayotov, M., Popa, I., 680 Rothe, A., Seftigen, K., Seim, A., Svarva, H., Svoboda, M., Thun, T., Timonen, M., Touchan, R., Trotsiuk, V., Trouet, V., Walder, F., Wążny, T., Wilson, R., and Zang, C.: Old World megadroughts and pluvials during the Common Era, *Science Advances*, 1, e1500561, <https://doi.org/10.1126/sciadv.1500561>, 2015.
- Cook, B. I., M. J. S. M. K. W. A. P. S. J. E. . A. K. J.: Twenty-first century drought projections in the CMIP6 forcing scenarios, *Earth’s Future*, 8, e2019EF001461, <https://doi.org/10.1029/2019EF001461>, 2020.
- 685 Cos, J., Doblas-Reyes, F., Jury, M., Marcos, R., Bretonnière, P.-A., and Samsó, M.: The Mediterranean climate change hotspot in the CMIP5 and CMIP6 projections, *Earth System Dynamics*, 13, 321–340, <https://doi.org/10.5194/esd-13-321-2022>, publisher: Copernicus GmbH, 2022.
- Dai, A.: Drought under global warming: a review, *Wiley Interdisciplinary Reviews: Climate Change*, 2, 45–65, <https://doi.org/10.1002/wcc.81>, 2011.
- 690 Dirmeyer, P. A.: The terrestrial segment of soil moisture–climate coupling, *Geophysical Research Letters*, 38, <https://doi.org/10.1029/2011GL048268>, eprint: <https://onlinelibrary.wiley.com/doi/pdf/10.1029/2011GL048268>, 2011.
- Douville, H., Raghavan, K., Renwick, J., Allan, R., Arias, P., Barlow, M., Cerezo-Mota, R., Cherchi, A., Gan, T., Gergis, J., Jiang, D., Khan, A., Pokam Mba, W., Rosenfeld, D., Tierney, J., and Zolina, O.: Water Cycle Changes. In *Climate Change 2021: The Physical Science Basis. Contribution of Working Group I to the Sixth Assessment Report of the Intergovernmental Panel on Climate Change*, Cambridge 695 University Press, Cambridge, United Kingdom and New York, NY, USA, p. 1513–1766, <https://doi.org/10.1017/9781009157896.010>, [Masson-Delmotte, V., P. Zhai, A. Pirani, S.L. Connors, C. Péan, S. Berger, N. Caud, Y. Chen, L. Goldfarb, M.I. Gomis, M. Huang, K. Leitzell, E. Lonnoy, J.B.R. Matthews, T.K. Maycock, T. Waterfield, O. Yelekçi, R. Yu, and B. Zhou (eds.)], 2021.

- Dubrovský, M., Hayes, M., Duce, P., Trnka, M., Svoboda, M., and Zara, P.: Multi-GCM projections of future drought and climate variability indicators for the Mediterranean region, *Regional Environmental Change*, 14, 1907–1919, <https://doi.org/10.1007/s10113-013-0562-z>, 2014.
- Düneloh, A. and Jacobeit, J.: Circulation dynamics of Mediterranean precipitation variability 1948–98, *International Journal of Climatology: A Journal of the Royal Meteorological Society*, 23, 1843–1866, <https://doi.org/10.1002/joc.973>, 2003.
- Esit, M., Kumar, S., Pandey, A., Lawrence, D. M., Rangwala, I., and Yeager, S.: Seasonal to multi-year soil moisture drought forecasting, *npj Climate and Atmospheric Science*, 4, 1–8, <https://doi.org/10.1038/s41612-021-00172-z>, number: 1 Publisher: Nature Publishing Group, 2021.
- Fang, L., Hain, C. R., Zhan, X., and Anderson, M. C.: An inter-comparison of soil moisture data products from satellite remote sensing and a land surface model, *International Journal of Applied Earth Observation and Geoinformation*, 48, 37–50, <https://doi.org/10.1016/j.jag.2015.10.006>, 2016.
- Gao, Y. and Gao, C.: European hydroclimate response to volcanic eruptions over the past nine centuries, *International Journal of Climatology*, 37, 4146–4157, <https://doi.org/10.1002/joc.5054>, 2017.
- Gent, P. R., Danabasoglu, G., Donner, L. J., Holland, M. M., Hunke, E. C., Jayne, S. R., Lawrence, D. M., Neale, R. B., Rasch, P. J., Vertenstein, M., Worley, P. H., Yang, Z.-L., and Zhang, M.: The community climate system model version 4, *Journal of climate*, 24, 4973–4991, <https://doi.org/10.1175/2011JCLI4083.1>, 2011.
- Ghannam, K., Nakai, T., Paschalis, A., Oishi, C. A., Kotani, A., Igarashi, Y., Kumagai, T., and Katul, G. G.: Persistence and memory timescales in root-zone soil moisture dynamics, *Water Resources Research*, 52, 1427–1445, <https://doi.org/10.1002/2015WR017983>, 2016.
- Giorgi, F.: Climate change hot-spots, *Geophysical research letters*, 33, <https://doi.org/10.1029/2006GL025734>, 2006.
- Grinsted, A., Moore, J. C., and Jevrejeva, S.: Application of the cross wavelet transform and wavelet coherence to geophysical time series, *Nonlinear Processes in Geophysics*, 11, 561–566, <https://hal.archives-ouvertes.fr/hal-00302394>, publisher: European Geosciences Union (EGU), 2004.
- Hagemann, S. and Stacke, T.: impact of the soil hydrology scheme on simulated soil moisture memory, *Climate Dynamics*, 44, 1731–1750, <https://doi.org/10.1007/s00382-014-2221-6>, 2015.
- Hannachi, A., Jolliffe, I. T., and Stephenson, D. B.: Empirical orthogonal functions and related techniques in atmospheric science: A review, *International Journal of Climatology*, 27, 1119–1152, <https://doi.org/https://doi.org/10.1002/joc.1499>, 2007.
- Haren, R. v., Haarsma, R. J., Oldenborgh, G. J. V., and Hazeleger, W.: Resolution Dependence of European Precipitation in a State-of-the-Art Atmospheric General Circulation Model, *Journal of Climate*, 28, 5134–5149, <https://doi.org/10.1175/JCLI-D-14-00279.1>, publisher: American Meteorological Society Section: *Journal of Climate*, 2015.
- Hersbach, H., Bell, B., Berrisford, P., Biavati, G., Horányi, A., Muñoz Sabater, J., Nicolas, J., Peubey, C., Radu, R., Rozum, I., et al.: ERA5 hourly data on single levels from 1979 to present, (Accessed on December 28, 2021), 10.24381/cds.adbb2d47, 2018.
- Hersbach, H., Bell, B., Berrisford, P., Hirahara, S., Horányi, A., Muñoz-Sabater, J., Nicolas, J., Peubey, C., Radu, R., Schepers, D., Simmons, A., Soci, C., Abdalla, S., Abellan, X., Balsamo, G., Bechtold, P., Biavati, G., Bidlot, J., Bonavita, M., Chiara, G. D., Dahlgren, P., Dee, D., Diamantakis, M., Dragani, R., Flemming, J., Forbes, R., Fuentes, M., Geer, A., Haimberger, L., Healy, S., Hogan, R. J., Hólm, E., Janisková, M., Keeley, S., Laloyaux, P., Lopez, P., Lupu, C., Radnoti, G., Rosnay, P. d., Rozum, I., Vamborg, F., Villaume, S., and Thépaut, J.-N.: The ERA5 global reanalysis, *Quarterly Journal of the Royal Meteorological Society*, 146, 1999–2049, <https://doi.org/https://doi.org/10.1002/qj.3803>, eprint: <https://rmets.onlinelibrary.wiley.com/doi/pdf/10.1002/qj.3803>, 2020.



- Huang, Y., Gerber, S., Huang, T., and Lichstein, J. W.: Evaluating the drought response of CMIP5 models using global gross primary productivity, leaf area, precipitation, and soil moisture data, *Global Biogeochemical Cycles*, 30, 1827–1846, <https://doi.org/10.1002/2016GB005480>, 2004.
- Iles, C. E. and Hegerl, G. C.: The global precipitation response to volcanic eruptions in the CMIP5 models, *Environmental Research Letters*, 740 9, 104012, <https://doi.org/10.1088/1748-9326/9/10/104012>, publisher: IOP Publishing, 2014.
- Kim, W. M. and Raible, C. C.: Dynamics of the Mediterranean droughts from 850 to 2099 CE in the Community Earth System Model, *Climate of the Past*, 17, 887–911, <https://doi.org/10.5194/cp-17-887-2021>, 2021.
- Kleidon, A.: Global datasets of rooting zone depth inferred from inverse methods, *Journal of Climate*, 17, 2714–2722, [https://doi.org/10.1175/1520-0442\(2004\)017<2714:GDORZD>2.0.CO;2](https://doi.org/10.1175/1520-0442(2004)017<2714:GDORZD>2.0.CO;2), 2004.
- 745 Kopparla, P., Fischer, E. M., Hannay, C., and Knutti, R.: Improved simulation of extreme precipitation in a high-resolution atmosphere model, *Geophysical Research Letters*, 40, 5803–5808, <https://doi.org/10.1002/2013GL057866>, 2013.
- Krichak, S. O. and Alpert, P.: Decadal trends in the east Atlantic–west Russia pattern and Mediterranean precipitation, *International journal of climatology: a journal of the Royal Meteorological Society*, 25, 183–192, <https://doi.org/10.1002/joc.1124>, 2005.
- Lehner, F., Joos, F., Raible, C. C., Mignot, J., Born, A., Keller, K. M., and Stocker, T. F.: Climate and carbon cycle dynamics in a CESM 750 simulation from 850 to 2100 CE, *Earth System Dynamics*, 6, 411–434, <https://doi.org/10.5194/esd-6-411-2015>, publisher: Copernicus GmbH, 2015.
- Lehner, F., Coats, S., Stocker, T. F., Pendergrass, A. G., Sanderson, B. M., Raible, C. C., and Smerdon, J. E.: Projected drought risk in 1.5 C and 2 C warmer climates, *Geophysical Research Letters*, 44, 7419–7428, <https://doi.org/10.1002/2017GL074117>, 2017.
- Lionello, P., Malanotte-Rizzoli, P., and Boscolo, R.: *Mediterranean Climate Variability*, Elsevier, 2006.
- 755 Maher, N., Matei, D., Milinski, S., and Marotzke, J.: ENSO change in climate projections: forced response or internal variability?, *Geophysical Research Letters*, 45, 11–390, <https://doi.org/10.1029/2018GL079764>, 2018.
- Markonis, Y., Hanel, M., Máca, P., Kyselý, J., and Cook, E. R.: Persistent multi-scale fluctuations shift European hydroclimate to its millennial boundaries, *Nature Communications*, 9, 1767, <https://doi.org/10.1038/s41467-018-04207-7>, 2018.
- Masson-Delmotte, V., Zhai, P., Pirani, A., Connors, S. L., Péan, C., Berger, S., Caud, N., Chen, Y., Goldfarb, L., Gomis, M., et al.: Climate 760 change 2021: the physical science basis, Contribution of working group I to the sixth assessment report of the intergovernmental panel on climate change, 2, 1513–1766, <https://doi.org/10.1017/9781009157896.013>, 2021.
- Monahan, A. H., Fyfe, J. C., Ambaum, M. H. P., Stephenson, D. B., and North, G. R.: Empirical Orthogonal Functions: The Medium is the Message, *Journal of Climate*, 22, 6501 – 6514, <https://doi.org/10.1175/2009JCLI3062.1>, 2009.
- Otto-Bliesner, B. L., Brady, E. C., Fasullo, J., Jahn, A., Landrum, L., Stevenson, S., Rosenbloom, N., Mai, A., and Strand, G.: Climate 765 Variability and Change since 850 CE: An Ensemble Approach with the Community Earth System Model, *Bulletin of the American Meteorological Society*, 97, 735–754, <https://doi.org/10.1175/BAMS-D-14-00233.1>, publisher: American Meteorological Society Section: Bulletin of the American Meteorological Society, 2016.
- PAGES Hydro2k Consortium et al.: Comparing proxy and model estimates of hydroclimate variability and change over the Common Era, *Climate of the Past*, 13, 1851–1900, 2017.
- 770 Previdi, M. and Liepert, B. G.: Annular modes and Hadley cell expansion under global warming, *Geophysical Research Letters*, 34, <https://doi.org/10.1029/2007GL031243>, 2007.

- Rao, M. P., Cook, B. I., Cook, E. R., D'Arrigo, R. D., Krusic, P. J., Anchukaitis, K. J., LeGrande, A. N., Buckley, B. M., Davi, N. K., Leland, C., and Griffin, K. L.: European and Mediterranean hydroclimate responses to tropical volcanic forcing over the last millennium, *Geophysical Research Letters*, 44, 5104–5112, <https://doi.org/10.1002/2017GL073057>, 2017.
- 775 Roberts, N., Moreno, A., Valero-Garcés, B. L., Corella, J. P., Jones, M., Allcock, S., Woodbridge, J., Morellón, M., Luterbacher, J., Xoplaki, E., et al.: Palaeolimnological evidence for an east–west climate see-saw in the Mediterranean since AD 900, *Global and Planetary Change*, 84, 23–34, <https://doi.org/10.1016/j.gloplacha.2011.11.002>, 2012.
- Rodell, M., Houser, P., Jambor, U., Gottschalck, J., Mitchell, K., Meng, C.-J., Arsenault, K., Cosgrove, B., Radakovich, J., Bosilovich, M., et al.: The global land data assimilation system, *Bulletin of the American Meteorological society*, 85, 381–394, <https://doi.org/10.1175/BAMS-85-3-381>, 2004.
- 780 Rodwell, M. J. and Hoskins, B. J.: Monsoons and the dynamics of deserts, *Quarterly Journal of the Royal Meteorological Society*, 122, 1385–1404, <https://doi.org/10.1002/qj.49712253408>, 1996.
- Samaniego, L., Thober, S., Kumar, R., Wanders, N., Rakovec, O., Pan, M., Zink, M., Sheffield, J., Wood, E. F., and Marx, A.: Anthropogenic warming exacerbates European soil moisture droughts, *Nature Climate Change*, 8, 421–426, <https://doi.org/10.1038/s41558-018-0138-5>, 2018.
- 785 Schmidt, G. A., Jungclaus, J. H., Ammann, C. M., Bard, E., Braconnot, P., Crowley, T. J., Delaygue, G., Joos, F., Krivova, N. A., Muscheler, R., Otto-Bliesner, B. L., Pongratz, J., Shindell, D. T., Solanki, S. K., Steinhilber, F., and Vieira, L. E. A.: Climate forcing reconstructions for use in PMIP simulations of the Last Millennium (v1.1), *Geoscientific Model Development*, pp. 185–191, <https://doi.org/https://doi.org/10.5194/gmd-5-185-2012>, 2012.
- 790 Schmidt, G. A., Kelley, M., Nazarenko, L., Ruedy, R., Russell, G. L., Aleinov, I., Bauer, M., Bauer, S. E., Bhat, M. K., Bleck, R., Canuto, V., Chen, Y.-H., Cheng, Y., Clune, T. L., Del Genio, A., de Fainchtein, R., Faluvegi, G., Hansen, J. E., Healy, R. J., Kiang, N. Y., Koch, D., Laxis, A. A., LeGrande, A. N., Lerner, J., Lo, K. K., Matthews, E. E., Menon, S., Miller, R. L., Oinas, V., Olosio, A. O., Perlwitz, J. P., Puma, M. J., Putman, W. M., Rind, D., Romanou, A., Sato, M., Shindell, D. T., Sun, S., Syed, R. A., Tausnev, N., Tsigaridis, K., Unger, N., Voulgarakis, A., Yao, M.-S., and Zhang, J.: Configuration and assessment of the GISS ModelE2 contributions to the CMIP5 archive, *Journal of Advances in Modeling Earth Systems*, 6, 141–184, <https://doi.org/10.1002/2013MS000265>, 2014.
- 795 Seneviratne, S., Zhang, X., Adnan, M., Badi, W., Dereczynski, C., Di Luca, A., Ghosh, S., Iskandar, I., Kossin, J., Lewis, S., Otto, F., Pinto, I., Satoh, M., Vicente-Serrano, S. M., Wehner, M., , and Zhou, B.: Weather and Climate Extreme Events in a Changing Climate. In *Climate Change 2021: The Physical Science Basis. Contribution of Working Group I to the Sixth Assessment Report of the Intergovernmental Panel on Climate Change*, Cambridge University Press, Cambridge, United Kingdom and New York, NY, USA, p. 1513–1766, <https://doi.org/10.1017/9781009157896.013>, [Masson-Delmotte, V., P. Zhai, A. Pirani, S.L. Connors, C. Péan, S. Berger, N. Caud, Y. Chen, L. Goldfarb, M.I. Gomis, M. Huang, K. Leitzell, E. Lonnoy, J.B.R. Matthews, T.K. Maycock, T. Waterfield, O. Yelekçi, R. Yu, and B. Zhou (eds.)], 2021.
- Shahapure, K. R. and Nicholas, C.: Cluster quality analysis using silhouette score, in: 2020 IEEE 7th International Conference on Data Science and Advanced Analytics (DSAA), pp. 747–748, IEEE, <https://ieeexplore.ieee.org/document/9260048>, 2020.
- 805 Spinoni, J., Barbosa, P., Buchignani, E., Cassano, J., Cavazos, T., Christensen, J. H., Christensen, O. B., Coppola, E., Evans, J., Geyer, B., et al.: Future global meteorological drought hot spots: a study based on CORDEX data, *Journal of Climate*, 33, 3635–3661, <https://doi.org/10.1175/JCLI-D-19-0084.1>, 2020.

- Stevenson, S., Fasullo, J. T., Otto-Bliesner, B. L., Tomas, R. A., and Gao, C.: Role of eruption season in reconciling model and proxy responses to tropical volcanism, *Proceedings of the National Academy of Sciences*, 114, 1822–1826, <https://doi.org/10.1073/pnas.1612505114>, publisher: Proceedings of the National Academy of Sciences, 2017.
- 810 Stockhecke, M., Timmermann, A., Kipfer, R., Haug, G. H., Kwiecien, O., Friedrich, T., Menviel, L., Litt, T., Pickarski, N., and Anselmetti, F. S.: Millennial to orbital-scale variations of drought intensity in the Eastern Mediterranean, *Quaternary Science Reviews*, 133, 77–95, <https://doi.org/10.1016/j.quascirev.2015.12.016>, 2016.
- Taylor, K. E., Stouffer, R. J., and Meehl, G. A.: An Overview of CMIP5 and the Experiment Design, *Bulletin of the American Meteorological Society*, 93, 485–498, <https://doi.org/10.1175/BAMS-D-11-00094.1>, 2012.
- 815 Trambly, Y., Koutroulis, A., Samaniego, L., Vicente-Serrano, S. M., Volaire, F., Boone, A., Le Page, M., Llasat, M. C., Albergel, C., Burak, S., Cailleret, M., Kalin, K. C., Davi, H., Dupuy, J.-L., Greve, P., Grillakis, M., Hanich, L., Jarlan, L., Martin-StPaul, N., Martínez-Vilalta, J., Mouillot, F., Pulido-Velazquez, D., Quintana-Seguí, P., Renard, D., Turco, M., Türkeş, M., Trigo, R., Vidal, J.-P., Vilagrosa, A., Zribi, M., and Polcher, J.: Challenges for drought assessment in the Mediterranean region under future climate scenarios, *Earth-Science Reviews*, 820 210, 103 348, <https://doi.org/10.1016/j.earscirev.2020.103348>, 2020.
- Tuel, A. and Eltahir, E. A.: Why is the Mediterranean a climate change hot spot?, *Journal of Climate*, 33, 5829–5843, <https://doi.org/10.1175/JCLI-D-19-0910.1>, 2020.
- Watanabe, S., Hajima, T., Sudo, K., Nagashima, T., Takemura, T., Okajima, H., Nozawa, T., Kawase, H., Abe, M., Yokohata, T., Ise, T., Sato, H., Kato, E., Takata, K., Emori, S., and Kawamiya, M.: The community climate system model version 4, *Geoscientific Model Development*, 4, 1063–1128, <https://doi.org/10.5194/gmd-4-845-2011>, 2011.
- 825 Wilks, D. S.: *Statistical methods in the atmospheric sciences*, vol. 100, Academic press, 2011.
- Wu, T., Song, L., Li, W., Wang, Z., Zhang, H., Xin, X., Zhang, Y., Zhang, L., Li, J., Wu, F., Liu, Y., Zhang, F., Shi, X., Chu, M., Zhang, J., Fang, Y., Wang, F., Lu, Y., Liu, X., Wei, M., Liu, Q., Zhou, W., Dong, M., Zhao, Q., Ji, J., Li, L., and Zhou, M.: An overview of BCC climate system model development and application for climate change studies, *Journal of Meteorological Research*, 28, 34–56, 830 <https://doi.org/10.1007/s13351-014-3041-7>, 2014.
- Wu, Y., Ting, M., Seager, R., Huang, H.-P., and Cane, M. A.: Changes in storm tracks and energy transports in a warmer climate simulated by the GFDL CM2. 1 model, *Climate dynamics*, 37, 53–72, <https://doi.org/10.1007/s00382-010-0776-4>, 2011.
- Xoplaki, E., González-Rouco, J., Luterbacher, J., and Wanner, H.: Wet season Mediterranean precipitation variability: influence of large-scale dynamics and trends, *Climate dynamics*, 23, 63–78, 2004.
- 835 Xoplaki, E., Trigo, R., García-Herrera, R., Barriopedro, D., D’andrea, F., Fischer, E., Gimeno, L., Gouveia, C., Hernández, E., Kuglitsch, F., et al.: Large-scale atmospheric circulation driving extreme climate events in the Mediterranean and related impacts (chapitre 6), <https://doi.org/10.1016/B978-0-12-416042-2.00006-9>, 2012.
- Xoplaki, E., Luterbacher, J., Wagner, S., Zorita, E., Fleitmann, D., Preiser-Kapeller, J., Sargent, A. M., White, S., Toreti, A., Haldon, J. F., Mordechai, L., Bozkurt, D., Akçer-Ön, S., and Izdebski, A.: Modelling Climate and Societal Resilience in the Eastern Mediterranean in the Last Millennium, *Human Ecology*, 46, 363–379, <https://doi.org/10.1007/s10745-018-9995-9>, 2018.
- 840 Yin, J. H.: A consistent poleward shift of the storm tracks in simulations of 21st century climate, *Geophysical Research Letters*, 32, <https://doi.org/10.1029/2005GL023684>, 2005.
- Zhou, S., Williams, A. P., Berg, A. M., Cook, B. I., Zhang, Y., Hagemann, S., Lorenz, R., Seneviratne, S. I., and Gentile, P.: Land–atmosphere feedbacks exacerbate concurrent soil drought and atmospheric aridity, *Proceedings of the National Academy of Sciences*, 116, 18 848–845 18 853, <https://doi.org/10.1073/pnas.1904955116>, publisher: National Academy of Sciences Section: Physical Sciences, 2019.

Zscheischler, J., Mahecha, M. D., and Harmeling, S.: Climate classifications: the value of unsupervised clustering, *Procedia Computer Science*, 9, 897–906, <https://doi.org/10.1016/j.procs.2012.04.096>, 2012.